EarthArXiv Coversheet

Francisco Ochoa[1,2], Philip G. Brodrick[2], Jorge A. Ochoa Gonzalez[3], Sandra LeGrand[3], Madeleine N. Gillespie[1], Red Willow Coleman[1,2], Yoseline Angel[4], K. Dana Chadwick[2], Regina F. Eckert[2], Kathleen Grant[2], Thoralf Meyer[5], David R. Thompson[2], Robert O. Green[2], Gregory S. Okin[1]

[1]Department of Geography, University of California Los Angeles, Los Angeles, CA, USA
[2]Jet Propulsion Laboratory, California Institute of Technology, Pasadena, CA, USA
[3]U.S. Army Engineer Research and Development Center, Geospatial Research Laboratory, Alexandria, VA, USA
[4]NASA Goddard Space Flight Center, Greenbelt, Maryland, USA
[5]Department of Geography, The University of Texas at Austin, Austin, TX, USA

fochoa1@g.ucla.edu

This pre-print was submitted for peer-review at *Remote Sensing of Environment.* The pre-print has not yet been peer-reviewed.

Evaluating global spectral unmixing techniques using imaging spectroscopy data for retrieval of green, non-photosynthetic vegetation, and soil fractional cover

Francisco Ochoa[1,2], Philip G. Brodrick[2], Jorge A. Ochoa Gonzalez[3], Sandra LeGrand[3], Madeleine N. Gillespie[1], Red Willow Coleman[1,2], Yoseline Angel[4], K. Dana Chadwick[2], Regina F. Eckert[2], Kathleen Grant[2], Thoralf Meyer[5], David R. Thompson[2], Robert O. Green[2], Gregory S. Okin[1]

[1]Department of Geography, University of California Los Angeles, Los Angeles, CA, USA
[2]Jet Propulsion Laboratory, California Institute of Technology, Pasadena, CA, USA
[3]U.S. Army Engineer Research and Development Center, Geospatial Research Laboratory, Alexandria, VA, USA
[4]NASA Goddard Space Flight Center, Greenbelt, Maryland, USA
[5]Department of Geography, The University of Texas at Austin, Austin, TX, USA

Keywords: spectral unmixing, imaging spectroscopy, E(MC)^2, MESMA, fractional cover, remote sensing.

Abstract

Global estimates of fractional cover of green vegetation (GV), non-photosynthetic vegetation (NPV), and soil provide valuable information about the Earth system. As the new generation of Earth visible-to-shortwave infrared (VSWIR) imaging spectrometers take orbit, global fractional cover data will be obtainable with new and improved spectral unmixing algorithms. Using an ASD Field Spectrometer and the spectral line point intercept (SLPIT) method, we estimate fractional cover from field measurements to compare to contemporaneous airborne (Airborne Visible/Infrared Imaging Spectrometer; AVIRIS$_{NG}$) and spaceborne (Earth surface Mineral dust source InvesTigation; EMIT) imaging spectroscopy data. Field data were collected in multiple biomes in the US Southwest at 84 validation sites. We used EndMember Combination Monte Carlo (E(MC)^2) and Multiple-Endmember Spectral Mixture Analysis (MESMA) to derive fractional cover, two candidate spectral unmixing algorithms used by current (e.g., EMIT) and future imaging spectroscopy missions. Field data exhibited strong agreement between ground and spaceborne/airborne measurements. Our best spectral unmixing approach, E(MC)^2, produced mean absolute error of ≤ 0.06 for NPV, GV, and soil with uncertainties ≤ 0.08 for all classes. We further investigated the performance of global vs. local endmember libraries and found that the global library outperformed the local endmember library. We investigated normalization techniques and their effectiveness with our ground and image fractions. Additionally, we calculated uncertainties from both ground and image fractions. Field results aligned well and within uncertainty predictions from previously reported simulation work. These findings support the use of E(MC)^2 to be used in current and future imaging spectroscopy missions.

1. Introduction

In the past three decades, imaging spectroscopy has been applied throughout the solar system, including the mapping of ancient lake beds on Mars (Amundson et al., 2008), mineral composition of the Moon's surface (Yan et al., 2010), and on Earth, mapping surface mineral features (Clark et al., 2022, 2003), methane sources (Thorpe et al., 2023), and vegetation (Angel et al., 2025; Ochoa et al., 2025b) with greater precision and accuracy than ever before.

On Earth, the quantification of global fractional cover of vegetation and soil at regular intervals via the visible-shortwave infrared (VSWIR, 350-2500 nm) portion of the electromagnetic spectrum would provide crucial information about terrestrial biomes.

Many studies have demonstrated the capability to derive fractional cover information using a variety of field measurements and remote observation. Spectral mixture analysis (SMA), also called spectral unmixing, is one of the fundamental methods for such fractional cover retrievals (Adams et al., 1986; Shimabukuro and Smith, 1991). In its simplest form, SMA uses a single spectrum of each ground component to unmix a remotely sensed spectrum of the surface. Multiple Endmember Spectral Mixture Analysis (MESMA) (Roberts et al., 1998) expanded SMA by allowing pixels to be unmixed by different endmember spectra, though each pixel could still be only unmixed by a single endmember spectrum for each ground cover component. Ochoa et al. (2025b) developed a global spectral unmixing algorithm to derive fractional cover, EndMember Combination Monte Carlo, $E(MC)^2$, which allows each pixel to be unmixed by multiple endmembers of each ground cover component in a Monte Carlo framework that also provides estimates of uncertainty. Linear spectral unmixing approaches are not the only way to estimate surface fractions. For example, several studies have used machine learning algorithms to derive fractional cover of vegetation and urban environments (Dennison et al., 2023; Schug et al., 2020, 2018; Senf et al., 2020; Wang et al., 2022).

Validation of fractional cover derived from spaceborne and airborne sensors presents unique challenges. Challenges that accompany any type of field validation work include geographic inaccuracies, site access, and the Modulation Transfer Function (Townshend et al., 2000). Several attempts have been made to validate remotely sensed fractional cover estimates *in situ*. Multiple studies have relied on transects (or quadrats) in which the user classifies a point as belonging to a class (Guerschman et al., 2015; Guerschman and Hill, 2018; Rigge et al., 2019; Scarth et al., 2015; Sutton et al., 2022; Wang et al., 2019). Other studies have used photo and image based approaches in which users or algorithms classify an *in situ* RGB or high resolution orthorectified image (Dennison and Roberts, 2003; Guerschman et al., 2009; Liu et al., 2019; Mu et al., 2015; Okin et al., 2013; Roberts et al., 1993; Tsendbazar et al., 2018). Promisingly, recent studies have coupled ground based imaging spectroscopy with spectral unmixing to quantify *in situ* fractional cover, finding improved agreement with remote sensing estimates from various sensors (Chadwick et al., 2025; Fisk et al., 2019b, 2019a; Meyer and Okin, 2015; Wang et al., 2019). The focus of this study is on the validation of linearly unmixed fractional cover estimates of green vegetation (GV), non-photosynthetic vegetation (NPV), and soil fractions from both spaceborne and airborne instruments using field measurements. The approach developed by Meyer and Okin (2015), the spectral line point intercept transect (SLPIT), was selected as the field measurement method of choice for our study as it enables a standardized and replicable method for validating fractional cover and has been successfully deployed in various global drylands (Fisk et al., 2019b, 2019a).

For this study, we use data from the Earth surface Mineral dust source InvesTigation (EMIT; Green et al., 2020; Thompson et al., 2024) imaging spectrometer (in orbit 2022 – present) and the Airborne Visible-InfraRed Imaging Spectrometer - Next Generation ($AVIRIS_{NG}$; Chapman et al., 2019). NASA's Surface Biology and Geology (SBG; Stavros et al., 2023; Thompson et al., 2020) mission is likely to incorporate a visible-shortwave infrared (VSWIR, 350-2500 nm) imaging spectrometer very similar to EMIT. Therefore, EMIT and

AVIRIS$_{NG}$ are an excellent validation case for fractional cover products for the next generation of global, sun-synchronous imaging spectrometers.

2. Methods

In this study, we collected *in situ* validation data of GV, NPV, and soil fractional cover at 84 field sites distributed throughout the Southwestern United States where airborne (AVIRIS$_{NG}$) and spaceborne (EMIT) imaging spectroscopy data were available. We describe a general approach of our field protocol in (Figure 1). We describe the collection and analysis of field data, as well as the approaches used to extract GV, NPV, and soil fractional cover from spaceborne and airborne imaging spectroscopy data. Error and uncertainty were then calculated between field and instrument derived estimates.

2.1 Field sites

A total of 84 field sites were visited in the southwest region of the United States (Figure 2). Each one of these sites were situated along EMIT orbital tracks (Green et al., 2020) or the Surface Biology Geology High Frequency Time Series (SHIFT) domain box (Figure 2; (Chadwick et al., 2025)), where AVIRIS$_{NG}$ data were acquired. 60 sites were in areas that were imaged by EMIT at ~60 m spatial resolution between February 2023 and November 2023. 24 sites were in areas imaged by AVIRIS$_{NG}$ at ~5 m spatial resolution between February 2022 and September 2022 as part of the SHIFT campaign (Chadwick et al., 2025). Due to the dynamic orbit pattern of the International Space Station, which hosts EMIT, field deployments were contingent upon the verification of a cloud-free scene, confirmed site accessibility, and favorable atmospheric and illumination conditions for field spectra collection. In most cases, field activities were conducted 0 to 10 days of data acquisition by either EMIT or AVIRIS$_{NG}$. Information on the sites' climate and vegetation can be found in Supplemental Table A.

2.2 Spectral line point intercept transects (SLPIT)

We used an approach for estimation of *in situ* fractional cover called spectral line point intercept transect (SLPIT) sampling, developed by Meyer and Okin (2015). SLPIT provides a way to estimate surface fractions of GV, NPV, and soil. SLPIT extends the line point intercept transect (LPIT) or point-based quadrat method. In LPIT, regularly spaced points along the transect (or in the quadrat) would be classified as belonging to GV, NPV, or soil. By definition, however, this approach struggles with mixtures at scales equivalent to the transect sampling interval, which are common in nature (Muir et al., 2011; Trevithick et al., 2012). These mixtures can result from spatial heterogeneity or physiological traits, such as plants with both GV and NPV tissues, green leaves with dead portions, or intermediate spectra from adaptations like sclerophyllous leaves or leaf hairs (Gitelson and Merzlyak, 1994; Okin, 2007). Thus, it can be slow for personnel and indistinguishable without additional equipment in the field to tell whether (and at what scale) a point along a traditional LPITs (or in quadrats) is best classed as GV or NPV (Fisk et al., 2019b, 2019a). Ambiguities can lead to subjective quantification of fractional cover and subsequent data inconsistency and inter-comparability issues. The classification problem is not limited just to discriminating between GV and NPV. Soil and NPV are often intimately mixed in real environments: leaves may be

covered with soil particles and soil is often a mixture of mineral components with plant litter (NPV).

SLPIT was developed to mitigate these conceptual as well as practical problems with traditional LPIT data collection when using the GV, NPV, and soil cover classes. In short, a SLPIT involves unmixing spectra (from a hand-held field spectrometer) taken along transect at regular intervals. Endmember spectra for this unmixing can be from anywhere (e.g., a global library) or can be made up of leaf-clip and contact-probe spectra from plants and soils in the immediate vicinity of the transect measurements (e.g., a local library). Additionally, because each spectrum along the transect is unmixed to estimate its fractional composition of the three endmembers, rather than assigning each point to a single class, an effort had been made to account for the multi-scale mixed nature of the cover types. Meyer and Okin (2015) and Fisk et al. (2019b, 2019a) showed that in structurally complex landscapes there was very little relationship between LPIT-derived fractions and satellite-derived fractions, but that satellite-derived fractions agreed well with SLPIT-derived fractions, likely due to considerations mentioned above. Therefore, we decided to use a version of their approach for this study, modified for the spatial resolution of EMIT and $\text{AVIRIS}_{\text{NG}}$ imagery.

The SLPIT method used here consisted of establishing three transects radiating from a central location (i.e., in a spoke arrangement) at each validation site. The spoke centers were at least 120 m from roads to minimize the potential for spectral contamination by unnatural surfaces. Each transect was 60 m long, and the orientation of the first transect was a perpendicular bearing to the sun's azimuth at the time of set up (≈ ±2 hours from solar noon). The remaining two transects were then separated by 120°. Each transect was sampled every 2.5 m with the bare fiber (FOV ~20°) using an ASD FieldSpec 4 Hi-Res NG Spectroradiometer (Malvern Panalytical, Malvern, hereafter referred to as "ASD") at approximately waist height (≈ 1 m), taking care to ensure that the measuring tape was not in the FOV. This approach results in a ground instantaneous field of view (GIFOV) of approximately 35 cm ensuring no overlap between points. Each transect had 25 individual spectra and thus the resulting cover for each validation point (each with 3 transects) was derived from a total of 75 spectra.

Because $\text{AVIRIS}_{\text{NG}}$ spatial sampling was much smaller than that of EMIT (5 m vs 60 m spatial resolution) and because we performed SLPIT immediately after the plant foliar trait sampling by Chadwick et al. (2025), we modified the spoked sampling strategy for these 24 AVIRIS_{NG} sites. For AVIRIS_{NG}, we used two 8-m north-south transects with their origins placed 2 m and 6 m along the east-west edge of an 8 m x 8 m sample plots. Each transect was sampled from waist height (≈ 1 m) every 0.33 m with the ASD fitted with an 8° FOV foreoptic, resulting in a GIFOV of approximately 14 cm ensuring no overlap between points. Each transect had 25 individual spectra and thus the resulting cover for each validation point (each with 2 transects) was derived from a total of 50 spectra.

A Spectralon™ (Labsphere, Sutton) panel was set up near the spoke center (e.g., for sites sampled with EMIT) or the edge of the 8 m x 8 m plot (e.g., for sites sampled with $\text{AVIRIS}_{\text{NG}}$) to collect white reference targets. White reference measurements were collected at the beginning and end of each transect to allow us to account for changes in illumination while sampling. Measurements always occurred within 2 hours of solar noon. Reflectance for SLPIT (for both EMIT and AVIRIS_{NG} sites) spectra (**r**) was obtained by dividing the radiance from the target measurements by radiance from the white reference targets. We also performed a temporal linear correction (independent for each wavelength) on **r** using,

$$\mathbf{r} = \frac{\mathbf{s}}{\mathbf{w_b} + \mathbf{m}(t - t_b)} \quad (1)$$

$$\mathbf{m} = \frac{\mathbf{w}_e - \mathbf{w}_b}{t_e - t_b}$$

where $\mathbf{s}$ represents the uncorrected spectra from SLPIT taken at time t, $\mathbf{m}$ is the slope calculated between changes of the white reference measurements collected at the beginning ($\mathbf{w_b}$) and end ($\mathbf{w_e}$) of each transect taken each at time t_e and t_b. The average time between measurements of $\mathbf{w_b}$ and $\mathbf{w_e}$ across all sites and transect lines was about 7 minutes. Furthermore, we corrected for light being absorbed by the Spectralon™ panel by multiplying $\mathbf{r}$ by a reference spectrum provided by the United States Geological Survey (Kokaly et al., 2017). To enable an accurate comparison between field and airborne/orbital measurements, SLPIT spectra were convolved to either EMIT or AVIRIS$_{NG}$ wavelengths. The spectra collected in this way were then unmixed using the approaches described below. Average fractional cover for a validation point was calculated as the average fractions from all the spectra taken at that point (75 for the EMIT spoked samples and 50 for the AVIRIS$_{NG}$ parallel transect samples). An example of spectra acquired from SLPIT can be found in (Figure 3).

2.3 Field endmember library collection

In situ spectral endmembers ($\mathbf{r_e}$) of GV, NPV, and soil were collected along/as close as possible to the SLPIT transects (Meyer and Okin, 2015) with an ASD contact probe (for NPV and soil) or leaf clip attachment (for GV). For EMIT sites, soil endmembers were collected using a contact probe every 2.5 m along the three 60 m spokes (75 total per site), and GV and NPV were collected with a leaf clip attachment (30 each per site). For AVIRIS$_{NG}$ sites, the number of endmembers collected ranged between 5-10 total for each endmember class due to the short length of the two 8 m transects and small area of the plot. Thus, for all AVIRIS$_{NG}$ sites, endmembers from the nearest sampled plots (either EMIT or AVIRIS$_{NG}$) were incorporated to ensure that each *in situ* endmember library set contained 30 GV, 30 NPV, and 75 soil spectra. Similarly, for EMIT sites lacking the required endmembers, endmembers from the nearest EMIT plots were used to meet the same criteria.

All *in situ* endmembers were visually inspected for known absorption features to avoid contamination issues: GV spectra must show chlorophyll and water absorptions; NPV spectra do not have strong chlorophyll absorptions and water absorption do not mask cellulose and lignin absorption features in the SWIR; soil spectra do not show strong liquid water or cellulose/lignin absorptions or also show some indication of absorption by iron oxide and/or clay minerals or else show no spectral absorption features other than a general increase in reflectance at longer wavelengths (Curran, 1989; Kokaly et al., 2017; Kokaly and Skidmore, 2015). Spectra that did not conform to these criteria were omitted from further use. These data served as local unmixing library set for their respective sites, resulting in 84 unique local endmember library sets (hereafter denoted with the subscript $_{local}$).

2.4 Imagery data and global library

Each validation point was within a recent EMIT or AVIRIS$_{NG}$ image. If multiple images were available, we chose the closest in time (Supplemental Table A). We used the Level 2A

Surface Reflectance product derived from EMIT and AVIRIS$_{NG}$ (Brodrick et al., 2025a; Green, 2022) and extracted a 3 x 3 pixel window centered on the pixel that contained the center of the sampling plot (denoted below as $\mathbf{r_s}$) following the methodology from Meyer and Okin (2015). Surface reflectance and atmospheric corrections were derived using an Optimal Estimation technique implemented through IsoFit (Brodrick et al., 2022; Thompson et al., 2018) for both instruments.

Ochoa et al. (2025b) used convex hulls constructed across multiple principal component space to build a globally representative spectral endmember library set for soils and randomly selected NPV and GV spectra. We employed this library built with a 4 dimensional convex hull set to also test its performance in the field (Ochoa et al., 2025a, 2024). This endmember library set is hereafter denoted with subscript $_{global}$. An example of imaging spectroscopy data used in this study can be found in (Figure 3).

2.5 Spectral unmixing

Two approaches were used for spectral unmixing of $\mathbf{r}$ and $\mathbf{r_s}$: MESMA (Roberts et al., 1998) and E(MC)^2 (Ochoa et al., 2025b). Both were used to determine the fractional cover of GV, NPV, and soil. For both approaches, bands where water vapor frequently obscures the reflectance retrievals were omitted for unmixing in the deep-water absorption regions (1320 – 1480 nm and 1780 – 2040 nm) as well as the longest wavelengths (> 2450 nm). This resulted in 207 out of 285 total wavelengths (m) for EMIT and 308 out of 425 for AVIRIS$_{NG}$ being used for unmixing. Ochoa et al. (2025b) found that adjustments for brightness using brightness normalization minimized errors across GV, NPV, and soil. We implemented this normalization technique by dividing each spectrum ($\mathbf{r}$, $\mathbf{r_s}$, $\mathbf{r_e}$ and $\mathbf{r_g}$) by the L2 norm. To evaluate the impact of this normalization, unmixing (on both E(MC)^2 and MESMA) was done without normalization as well. We also implemented the recommended 25 Monte Carlo simulations associated with E(MC)^2 and MESMA for better performance and uncertainty calculations (Ochoa et al., 2025b). Both of these approaches use an unmixing matrix, **X.**

E(MC)^2 unmixed $\mathbf{r}$ and $\mathbf{r_s}$ using an unmixing matrix ($\mathbf{X_{local}}$ or $\mathbf{X_{global}}$), constructed from the endmember library set (section 2.3-2.4). The unmixing matrix was required to have at least one type of each endmember (GV, NPV, and soil), but each type could be represented more than once. We generated this unmixing library with 20 endmembers. In this 20-endmember case, 6 endmembers from each of the three classes were randomly chosen, and 2 endmember spectra were chosen randomly from the respective unmixing library sets, taking care to not include any endmember more than once.

MESMA differs from E(MC)^2 in that more combinations of fewer endmembers are used in the unmixing process. In MESMA, each target spectrum, $\mathbf{r}$ (or $\mathbf{r_s}$), is unmixed by each model,

$$\mathbf{X} \cdot \hat{\mathbf{f}} = \begin{bmatrix} x_0^{(npv)} & x_0^{(gv)} & x_0^{(soil)} \\ \vdots & \vdots & \vdots \\ x_m^{(npv)} & x_m^{(gv)} & x_m^{(soil)} \end{bmatrix} \cdot \begin{bmatrix} \hat{f}_{npv} \\ \hat{f}_{gv} \\ \hat{f}_{soil} \end{bmatrix} = \begin{bmatrix} r_0 \\ \vdots \\ r_m \end{bmatrix} = \mathbf{r}, \quad (2)$$

where only one spectrum each of GV, NPV, and soil allowed in the unmixing matrix $\mathbf{X_{local}}$ (or $\mathbf{X_{global}}$). The best-fit model is chosen as the one which minimizes the spectral root mean squared error (RMSE) (Roberts et al., 1998). Here, we set the number of models available (j) or MESMA to 100 based on the recommendations by Ochoa et al. (2025b).

2.6 Error metrics

Mean Absolute Error (MAE) and RMSE were calculated from the ground fractions (**f**; derived from **r**) and spaceborne/airborne fractions ($\hat{\mathbf{f}}$; derived from $\mathbf{r_s}$). Mean uncertainty ($M\bar{U}_T$; Equation 3) were calculated from the ground fractions ($\bar{u}_f$; derived from **r**) and spaceborne/airborne fractions ($\bar{u}_{\hat{f}}$; derived from $\mathbf{r_s}$), from MESMA and E(MC)^2 using,

$$M\bar{U}_T = \frac{1}{2N}\left\|\bar{u}_{\hat{f},k} + \bar{u}_{f,k}\right\|_1 \quad (3)$$

$$RMS\bar{U}_T = \frac{1}{2\sqrt{N}}\left\|\bar{u}_{\hat{f},k} + \bar{u}_{f,k}\right\|_2 \quad (4)$$

where N is the total number of sites and $_k$ refers to ground cover class (GV, NPV, soil).

3. Results

Overall, errors calculated between **f** and $\hat{\mathbf{f}}$ were low for each endmember cover class, with MAE ≤ 0.09 across all unmixing cases (Figure 4). Errors in GV fraction were lower than those for soil and NPV regardless of the unmixing case. For NPV and soil, sites that were unmixed with the global unmixing library set produced lower errors than their local unmixing library set counterpart, regardless of whether fractions were derived by E(MC)^2 or MESMA. All endmembers showed strong correlations between **f** and $\hat{\mathbf{f}}$ and values of $M\bar{U}_T$ were low (Table 1), though $M\bar{U}_T$ was higher in the global unmixing cases than the local. No systematic differences between EMIT and AVIRIS$_{NG}$ sites were observed (Table 1). The time between SLPIT data acquisition and coinciding airborne/spaceborne image acquisitions varied from -90 (e.g., days before overpass) to +65 (e.g., days after overpass) days with a mean of 6.5 days (e.g., days after overpass). There was no relationship between error and the number of days between SLPIT field sampling and image data acquisition (Supplemental Figure A). The performance of E(MC)^2 using the average of the 25 Monte Carlo runs showed better performance than the optimal solution (e.g., run with lowest spectral error) (Supplemental Figure B).

Brightness normalization had a minimal effect on estimated fraction retrievals of all classes. Differences in MAE between the two cases (brightness normalization and no normalization) were ≈≤ 0.01 for all unmixing cases and linearity (R^2) remained constant (not shown). Similarly, normalization did not impact $\overline{U}$. Because brightness normalization resulted in nearly identical error compared to no normalization for both E(MC)^2 and MESMA, further results display the result of unmixing using brightness normalization.

We investigated whether the agreement between SLPIT- and image-based fractions was because they were unmixed using the same approach (Figure 4) by comparing E(MC)^2-derived image fractions with MESMA-derived SLPIT fractions (Figure 6). Although MAE and RMSE in this comparison is slightly higher (0.01 – 0.03), there is still excellent agreement between the two, however, $\overline{U}$ was higher in E(MC)^2 than MESMA. We obtain the same result when comparing MESMA-derived image fractions with E(MC)^2-derived SLPIT fractions (not shown).

We further investigated whether agreement for both E(MC)^2 and MESMA was dependent on normalization of either field or remote data (Figure 7-8). E(MC)^2 MAE and RMSE showed excellent agreement between the two (Figure 7), thus indicating that agreement between field or remote data was not dependent on normalization. Furthermore, E(MC)^2 MAE (Figure 7) was almost identical or slightly higher (< 0.01) than the comparison when both image and SLPIT fractions are normalized (Figure 4). In contrast, MESMA was more dependent on normalization (Figure 8), as indicated by the slightly higher MAE and RMSE, particularly in the soil and NPV classes. MESMA MAE (from MESMA normalized vs. MESMA not-normalized) was also slightly higher (< 0.01) than the comparison when both image and SLPIT fractions were normalized.

We assessed whether the different solar geometries impact correspondence between these SLPIT- and image-derived fractions. AVIRIS$_{NG}$ is flown close to solar noon and therefore does not have a wide range of solar zenith angles (SZA) and was not included in this analysis but EMIT can acquire images with SZA up to 60°. However, no relationship was observed between fractional cover absolute error and EMIT SZA (Figure 5).

Table 1: Fractional cover error and uncertainty of different unmixing cases.

			NPV				*GV*				*SOIL*			
Algorithm	Case	Sensor*	MAE	RMSE	$M\bar{U}_T$	$RMS\bar{U}_T$	MAE	RMSE	$M\bar{U}_T$	$RMS\bar{U}_T$	MAE	RMSE	$M\bar{U}_T$	$RMS\bar{U}_T$
E(MC)^2	$_{local}$	EMIT	0.08	0.10	0.04	0.06	0.04	0.07	0.01	0.02	0.10	0.13	0.03	0.05
		AVIRIS$_{ng}$	0.09	0.11	0.05	0.08	0.04	0.06	0.02	0.03	0.08	0.10	0.04	0.06
		Combined	0.08	0.10	0.04	0.06	0.04	0.06	0.02	0.03	0.09	0.12	0.03	0.06
	$_{global}$	EMIT	0.06	0.07	0.07	0.11	0.05	0.07	0.02	0.03	0.04	0.05	0.07	0.10
		AVIRIS$_{ng}$	0.04	0.05	0.09	0.14	0.04	0.06	0.02	0.03	0.03	0.03	0.09	0.13
		Combined	0.06	0.07	0.08	0.12	0.04	0.07	0.02	0.03	0.04	0.05	0.08	0.11
MESMA	$_{local}$	EMIT	0.08	0.09	0.03	0.04	0.04	0.06	0.01	0.02	0.09	0.12	0.02	0.04
		AVIRIS$_{ng}$	0.09	0.11	0.03	0.04	0.04	0.06	0.01	0.02	0.09	0.12	0.02	0.04
		Combined	0.08	0.10	0.03	0.04	0.04	0.06	0.01	0.02	0.09	0.12	0.02	0.04
	$_{global}$	EMIT	0.08	0.09	0.06	0.08	0.05	0.07	0.02	0.03	0.07	0.09	0.06	0.08
		AVIRIS$_{ng}$	0.06	0.08	0.07	0.10	0.03	0.05	0.02	0.03	0.05	0.06	0.07	0.10
		Combined	0.07	0.09	0.06	0.09	0.04	0.06	0.02	0.03	0.06	0.08	0.06	0.09

*EMIT calculations are based on 60 sites. AVRIRIS$_{NG}$ calculations are based on 24 sites.

4. Discussion

As with many other unmixing studies using GV, NPV, and soil, GV fractions were retrieved with lower error than NPV and soil (Figure 4; Dennison et al., 2023, 2019; Guerschman et al., 2012; Meyer and Okin, 2015; Ochoa et al., 2025b; Okin et al., 2001). This results mainly from the fact that GV has distinctive spectral features (e.g., chlorophyll absorption, red edge, water absorptions) whereas NPV and soil tend have similar and potentially confounding spectral features (Asner and Heidebrecht, 2002; Meyer and Okin, 2015; Numata et al., 2008; Okin et al., 2001). NPV and soil can undergo spectral "coupling" when NPV endmembers lack the

distinct spectral features associated with GV, giving them a closer resemblance to soil and making a mixture of one spectra of each nearly indistinguishable from a different combination of spectra from each class (Okin et al., 2001).

Regardless, the results from this field study are slightly better and comparable to other studies that use imaging spectroscopy data for fractional cover estimation (Dennison et al., 2023, 2019; Ochoa et al., 2025b). The SZA collection window that Ochoa et al. (2025b) predicted was also verified by our studies, as no significant correlations between absolute error and SZA was found regardless of the unmixing cases for EMIT sites (Figure 5).

4.1 The use of SLPIT validation for fractional cover estimates

SLPIT has several advantages over more traditional methods of estimating fractional cover (e.g., LPIT, quadrat sampling) as it fundamentally relies on explicit spectral absorptions. A traditional LPIT approach requires the user to make dozens of judgments, per transect, on whether a point belongs to the GV, NPV, or soil class, even when detailed protocols are in place to ensure that just a single point is being read (Fisk et al., 2019b, 2019a; Guerschman et al., 2015; Guerschman and Hill, 2018; Meyer and Okin, 2015; Muir et al., 2011; Okin et al., 2013; Trevithick et al., 2012). Even at a single point, judgments are necessarily subjective. Because GV and NPV are intermixed at a variety of scales, this subjectivity can bias results and lead to inconsistencies between measurements made by different people. Furthermore, because litter (NPV) is intermixed with soils, there can also be the potential for NPV and soil to be confused in the subjective judgments of individuals making measurements. The problem is only partly a scale problem (GV/NPV and NPV/soil are intermixed at a variety of scales). Humans can only see in the visible range of the electromagnetic spectrum, yet some of the spectral features that distinguish between GV, NPV, and soil are outside the visible range (e.g., water, cellulose/lignin absorptions, metal-hydroxide mineral absorption features). Thus, a field technician may make a determination on the basis of color in the visible that is contradicted by spectral information in the infrared. For example, a fragment of a leaf may lack chlorophyll due to water stress or disease and thus be classified as NPV, and yet due to the presence of leaf water, may not exhibit the cellulose and lignin absorption features, that are characteristic of NPV. Is this sample classified best as GV, NPV, or something in between? Our purpose here isn't to make this determination, but rather to suggest that by using different spectral ranges, a human and a VSWIR imaging spectrometer may disagree on what class best suits a particular sample and, further, that the human's visible-range determination is as likely to be 'wrong' in an objective sense as the determination using VSWIR range.

In truth, the definition of GV, NPV, and soil classes are abstractions and some locations defy straightforward classification (e.g., Okin, 2007). This is common in remote sensing retrievals but exacerbated by the fine-scale (sometimes sub centimeter) spatial variability of GV, NPV, and soil. Thus, SLPIT is well suited for field estimates of GV, NPV, and soil fractional cover; it helps mitigate the subjectivity from field measurement and creates an objective basis from which ground "truth" might be determined. Furthermore, in cases where careful comparison of field-based fractional cover using traditional methods has been tried (e.g., Fisk et al. (2019b; Meyer and Okin (2015); Okin et al. (2013)), it was shown that these do not necessarily have any correspondence to what is seen by remote sensing instruments.

Due to the conceptual and practical difficulties of using traditional methods such as LPIT (or quadrat) for fractional cover ground validation, SLPITs are a reasonable option for

validating airborne- and space-based estimates of GV, NPV, and soil cover. Here, we validated two instruments (AVIRIS$_{NG}$ and EMIT) with different spectral sampling (5 nm and 7.5 nm, respectively) and spatial resolutions (5 m and 60 m, respectively). Hereafter, SLPIT fractional covers will be treated as "ground truth." An objection to the use of SLPIT may be the perceived circularity from using unmixing of ground spectra to validate unmixing of spectra from imaging spectrometers. We acknowledge the appearance of circularity here, but do not believe that it invalidates the utility of SLPITs for validation of GV, NPV, and soil fractions from unmixing of remotely sensed data. Fundamentally, we are conducting an instrument-to-instrument comparison where the SLPIT data are not subject to atmospheric correction and indirect reflectance inversion, while EMIT and AVIRIS$_{NG}$ data are (Brodrick et al., 2022; Thompson et al., 2018). There is certainly room for evaluating SLIPTs against more traditional methods, but it is outside the scope of the present study. To the knowledge of the authors, there is as of yet no standard method for acquisitions of fractional cover data.

4.2 Comparison to previous spectral unmixing studies (GV, NPV, Soil)

Ochoa et al. (2025b), Dennison et al. (2019), and Dennison et al. (2023) used simulations to understand the efficacy of spectral unmixing algorithms. Using the equivalent of the 'global' library used here, Ochoa et al. (2025b) produced estimates of fractional cover with MAE of NPV, GV, and soil cover in a simulation context of 0.10, 0.06, and 0.10, respectively, for E(MC)^2 and slightly higher for MESMA. Our field results provided estimates with MAE <0.08, 0.04, and 0.09 for the same classes. Dennison et al. (2019) used a simulation approach reported an NPV RMSE of 0.16, GV RMSE of 0.15, and soil RMSE of 0.14 with MESMA. Using different endmembers as well as implementation of a Monte Carlo element, our study produced a lower RMSE for NPV (0.09-0.10), GV (0.06), and soil (0.08-0.12) for MESMA.

Although Ochoa et al. (2025b) investigated the impact of SZA, water vapor, and aerosols, they simulated spectra without any vegetation structural complexity (e.g., canopy). At the outset of this study, we expected that vegetation canopy effects in the field would lead to larger errors compared to those simulated by Ochoa et al. (2025b). However, the results from the present study indicate that it is possible to obtain errors that are as good (in fact, slightly lower) when comparing image-derived and *in situ* estimates of fractional cover for the three ground cover components of interest here (Figure 4). We believe that this observed result is likely due to: (1) a favorable agreement was observed between SLPIT and spaceborne/airborne surface reflectance (MAE for reflectance was not calculated in our study, however, low errors were observed by Coleman et al. (2024) using some of our SLPIT data) (2) vegetation canopy effects were minimal on both SLPIT and spaceborne/airborne fractions as the majority of SLPIT measurements were taken ~ 1m above the ground, thus, the path length of photons going through the canopy was relative small across the majority of plots (3) the endmembers collected in our study and those used by Ochoa et al. (2025b) were likely influenced by non-linear scattering effects (e.g., stacked vegetation material measured by a leaf clip/contact probe could be contributing to increased spectra magnitudes), therefore our imaging spectroscopy data (SLPIT and imagery) which likely has non-linear effects were unmixed with a spectral unmixing library that likely had non-linear effects.

The fractional cover estimates from Fisk et al. (2019b) and Meyer and Okin (2015) used SLPIT, but were constrained to MODIS and Landsat wavelengths. Therefore, these data are not directly comparable with imaging spectrometer data. However, Asner and Heidebrecht

(2002) used a similar field and unmixing approach with AVIRIS$_{Classic}$ and found that values of soil cover were overestimated by 20%. In contrast, we found a better agreement for soil in all of our spectral unmixing cases, though our estimates of soil were underestimated using the local unmixing library sets.

Daughtry & Hunt (2008) estimated NPV cover using the cellulose absorption index through spectra collected from an older ASD spectrometer and reported an RMSE of 0.14 by comparing estimates to field photographs collected data in agricultural regions. Similarly, Dennison et al. (2023) retrieved NPV cover using a series of indices and reported RMSE between 0.14-0.16 for only this class. Our field study produced a slightly lower NPV RMSE for E(MC)^2 (0.07-0.10) and MESMA (0.09-0.10). Ochoa et al. (2025b)'s study, though simulation based, produced a slightly higher NPV RMSE for E(MC)^2 (0.12) and MESMA (0.15). Gill & Phinn (2008) and Gill & Phinn (2009) provided an RMSE (0.10 and 0.04, respectively) for soil, based on 38 and 12 field sites, respectively and with Advanced Thermal Emission and Reflection Radiometer (ASTER) data. Our field study produced soil RMSE for E(MC)^2 (0.05-0.12) and MESMA (0.08-0.12). They do not provide information on the GV or NPV class.

These comparisons indicate that the results presented here are in family with previous work, though generally perform slightly better. We hypothesize this is due to some combination of EMIT's and AVIRIS$_{NG}$ data quality, improvement in atmospheric correction, and the extent of the field work leveraged here.

4.3 Global vs. local endmember libraries, normalization, and multiple scattering

Meyer and Okin (2015) found that unmixing spectra with a local library improved retrievals compared to using a more general 'global' library. In contrast, our results indicate that using a global library actually improved estimates (reduced errors) for fractional cover retrievals of GV, NPV, and soil. The 'global' library of soils and vegetation endmembers used in the present study expanded off of those Meyer and Okin (2015), and is now considerably more diverse, which may contribute to this difference in performance. Future studies will help determine how generally this pattern holds, as global libraries continue to grow and diversify.

Scale-dependent impacts of structure on apparent brightness in vegetated systems are well described in the literature (Asner et al., 2000; Dennison et al., 2004; Dennison and Roberts, 2003; Ochoa et al., 2025b). Spectra of individual leaves tend to be brighter than those of branches and canopies due to self-shading and shading of the soil by vegetation canopies tends to darken the IFOV. Normalization, these authors argued, would help account for this scale-dependent brightness, especially in structurally complex vegetation. We therefore anticipated that when compared against field data, brightness normalization would also result in better results (lower error). However, our results show that normalization had a minimal effect on error rates, at least when using SLPIT to compare against image retrievals derived with E(MC)^2. We find this a somewhat surprising result given that our field sites span a range of vegetation structural complexity (Supplementary Table A). It is possible that this is a result of the dryland focus of this study, and that the presence of large trees in savannas or woodlands might alter the conclusion. The effect of normalization is slightly higher when using MESMA than E(MC)^2, but still small (Figure 8). This decrease in agreement (higher error) between E(MC)^2 and MESMA (Figure 7 vs. Figure

8) is probably due to the spectral magnitude of soil and NPV used by MESMA models. In this work, spectral normalization stands in for the retrieval of a 'shade fraction' and is in many ways analogous to Roberts et al. (1998). This research raises the possibility that it may be possible to avoid spectral normalization altogether, given high quality remote measurements and a diverse enough endmember library, though we do not make this claim in the absolute.

Several studies have demonstrated that complex vegetation canopies can introduce errors due to non-linear mixing (Czekajlo et al., 2021; Ray and Murray, 1996; Roberts et al., 1993). Ray and Murray (1996) demonstrated with field experiments that linear mixtures could overestimate vegetation fractions of *Larrea tridentata* (vegetation we observed at multiple of our sites) by 60%. Similarly, Czekajlo et al. (2021) also found that complex vegetation canopies in urban areas influence the amount of GV fractions being produced by linear unmixing of multi-spectral imagery. Nonlinear mixing of the spectral signal (mainly due to multiple interactions between the light and complex surface) would be expected to lead to increased unmixing error. We did not observe any impact of this in our results, perhaps because non-linear interactions would be present in both SLPIT and image data, but more likely because the field sites here did not include vegetation with large canopies.

4.4 Common sources of error

Comparing *in situ* and remote sensing data provides notorious scaling challenges. Our study had two different spatial scales: 60 m EMIT pixels and 5 m AVIRIS$_{NG}$. Therefore, the scale and total number of measurements per spectral transect differed fundamentally between these two instruments. Geographic inaccuracies of ground and spaceborne/airborne measurements also account for other challenges, however, in this study the geolocation error was not calculated. While Townshend et al. (2000) demonstrated that the signal that composes a pixel includes a proportion of signal originating from surrounding pixels due to many factors such as optics, detector, electronics, and/or atmospheric effects (e.g., Modulation Transfer Function), our study did not quantify this effect. Our endmember spectrum classification method is based on using key visual diagnostic features to label NPV, GV, and soil. At the limit, small impurities may not be caught through visual inspection or through diagnostic features. In those cases, some small percentage of error might be present in the endmember themselves. Furthermore, we recognize that these three ground cover classifications (NPV, GV, and soil) are a good abstraction for arid lands, but this abstraction ignores the complexities of urban, ice, water, and burned cover areas.

5. Conclusion

Our study found that E(MC)^2 and MESMA, as implemented here, produce fractional cover estimates with errors below 0.09 MAE and 0.12 RMSE across multiple biomes of the US southwest for GV, NPV, and soil, with E(MC)^2 having slightly better performance than MESMA. Both algorithms showed excellent agreement regardless of the imagery's spatial scale or wavelength differences. Some amount of spectral confusion between NPV and soil remained and could be exacerbated in areas with more exposed surface rocks or different minerology. Brightness normalization and solar zenith angle were shown to have minimal impact on the fractional cover retrievals. Uncertainties ($M\bar{U}_T$) originating from the Monte

Carlo runs also were below 0.09. The use of a global library forged by Ochoa et al. (2025b) performed slightly better than the use of *in situ* local endmembers. Even with these limitations, the errors, biases, uncertainties, and linearities were still found to be acceptable and aligned with the errors predicted in simulation (Ochoa et al., 2025b).

Our results also helped validate the spectral unmixing recommendations that Ochoa et al. (2025b) produced and helped forged our field protocols for SLPIT. Promisingly, it appears possible to obtain global fractional cover with EMIT using $E(MC)^2$. As future imaging spectroscopy missions take orbit (e.g., Surface Biology Geology (SBG); (Green et al., 2022), Copernicus Hyperspectral Imaging Mission for the Environment (CHIME); (Nieke et al., 2023)), there is growing potential to achieve global quantification of fractional cover at a regular interval, providing better insight of multiple biomes across the Earth's surface. This validation set serves to better our understanding of Earth's ecosystems in complex vegetated sites. We remained committed to open-source science and have made all study data and code available (Brodrick et al., 2025b; Ochoa et al., 2026, 2025a).

6. Acknowledgments

EMIT work was supported by the National Aeronautics and Space Administration Earth Venture Instrument program, under the Earth Science Division of the Science Mission Directorate. A portion of this research was performed at the Jet Propulsion Laboratory, California Institute of Technology, under a contract with the National Aeronautics and Space Administration. We acknowledge the exceptional support and assistance of NASA's International Space Station Program. A portion of this work was supported by the Future Investigators in NASA Earth and Space Science and Technology (FINESST) grant [80NSSC21K1621]. This research was supported by the U.S. Army Corps of Engineers (USACE), Engineer Research and Development Center (ERDC). Permission to publish was granted by the ERDC Public Affairs Office. The use of trade, product, or firm names in this document is for descriptive purposes only and does not imply endorsement by the U.S. Government. US Government Support Acknowledged.

7. CRedit

Francisco Ochoa: Writing - Original Draft, Methodology, Formal Analysis, Visualization, Validation, Data curation, Software. **Philip G. Brodrick**: Conceptualization, Writing - Review & Editing, Methodology, Resources, Software. **Jorge A. Ochoa Gonzalez:** Investigation, Writing - Review & Editing. **Sandra LeGrand**: Investigation, Resources. **Madeline N. Gillespie**: Investigation. **Red Willow Coleman**: Investigation, Writing - Review & Editing. **Yoseline Angel**: Investigation. **Dana K. Chadwick**: Investigation, Resources. **Regina F. Eckert**: Investigation. **Kathleen Grant:** Investigation, Writing - Review & Editing. **Thoralf Meyer:** Investigation, Writing - Review & Editing. **David R. Thompson**: Investigation, Resources, Software. **Robert O. Green**: Supervision, Funding Acquisition, Resources. **Gregory S. Okin**: Conceptualization, Funding Acquisition, Writing - Review & Editing, Resources, Supervision.

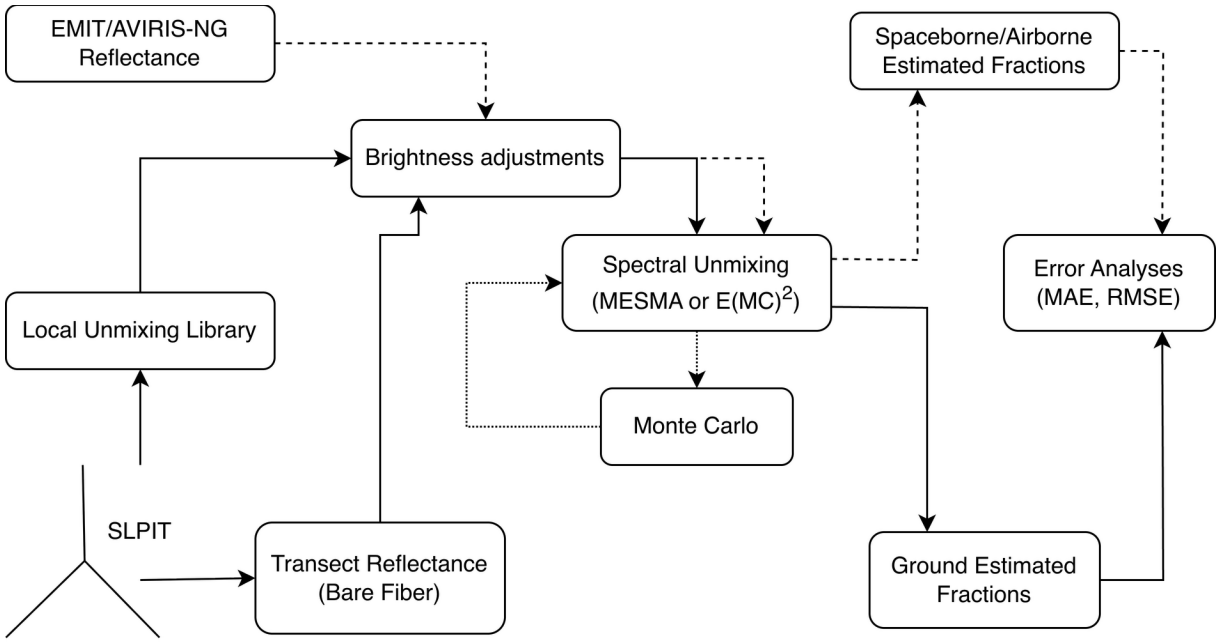

Figure 1: Workflow for calculating error of spectral unmixing from SLPIT field points and EMIT or AVIRIS-NG reflectance data.

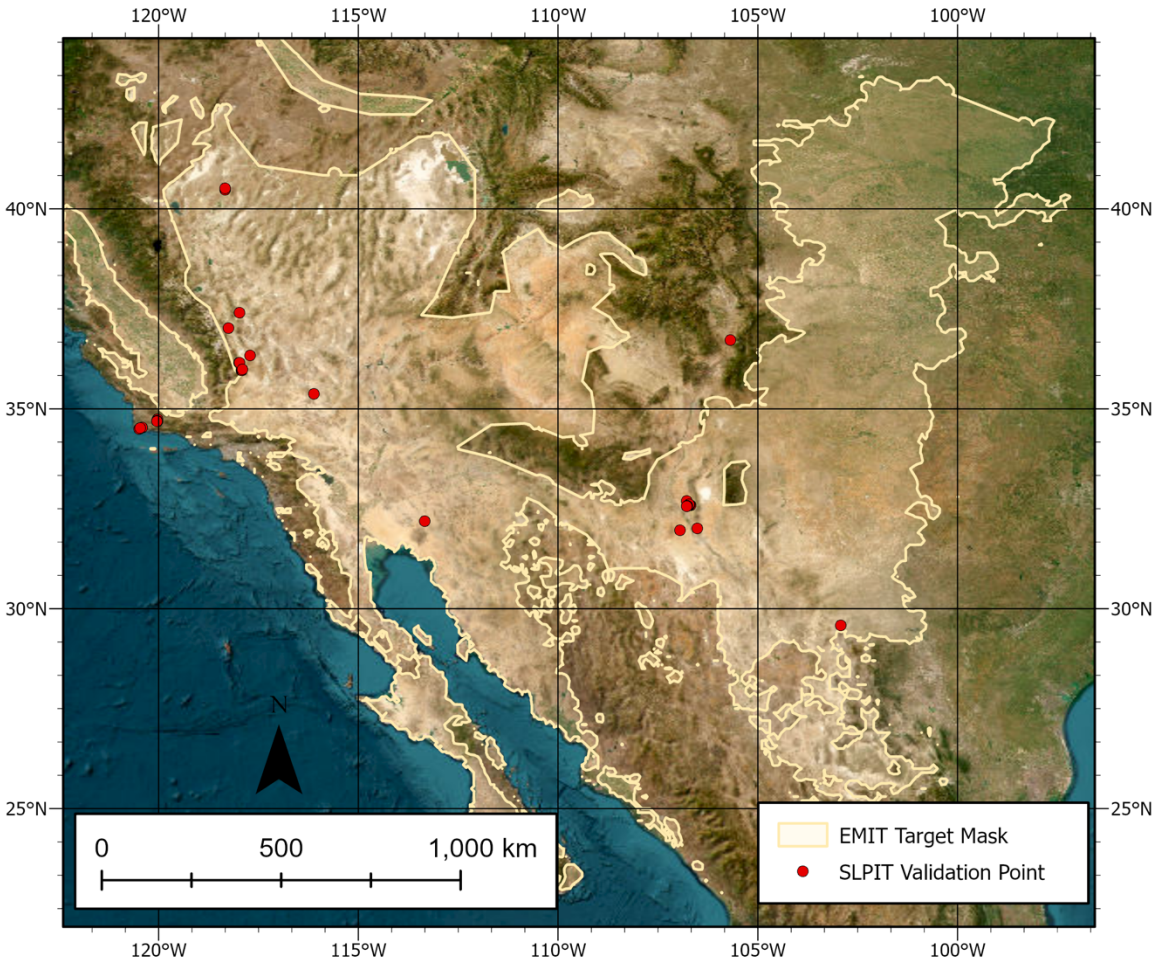

Figure 2: Location of SLPIT points used in this study. EMIT target acquisition mask from the prime mission (2022-2023) is shown by the yellow shaded polygon.

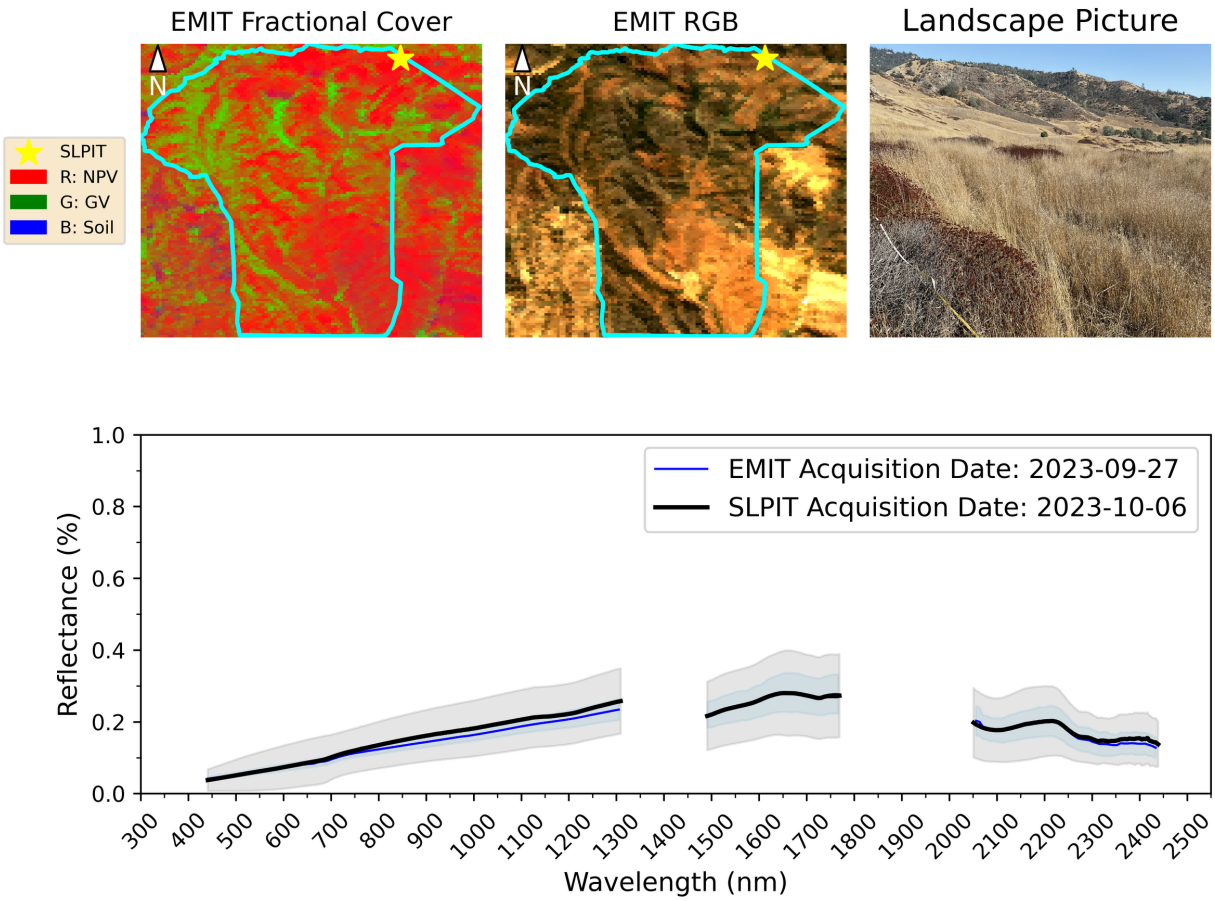

Figure 3: Top: EMIT fractional cover and true color RGB over Sedgwick Reserve, CA (acquired on 2023-09-27) with a corresponding selected SLPIT site ground view (acquired on 2023-10-06). Star symbol denotes selected SLPIT location. Bottom: Comparison of average reflectance measurements from SLPIT and EMIT.

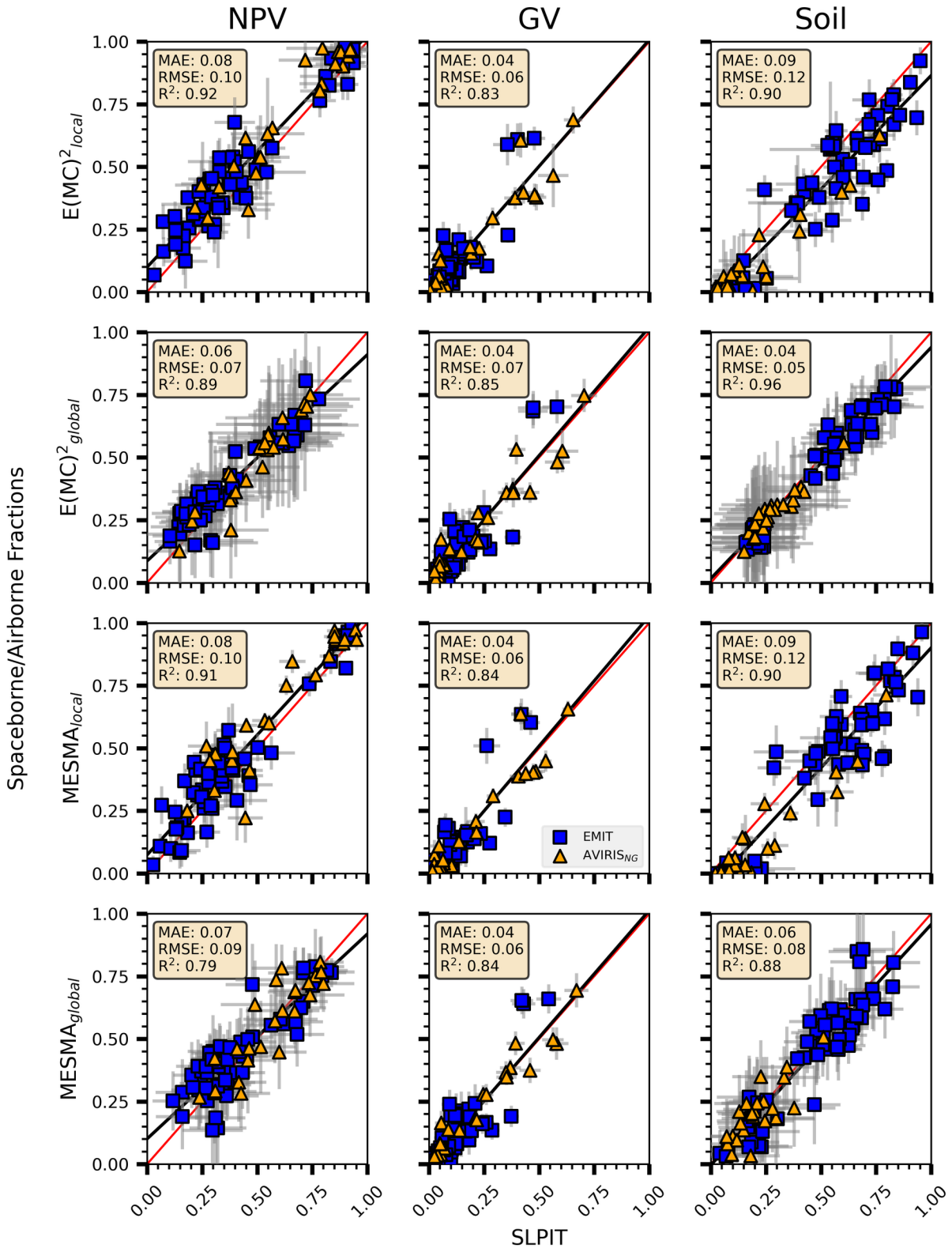

Figure 4: Comparison (n=84) of NPV, GV, and soil fractions estimated from SLPIT and EMIT/AVIRIS$_{NG}$ using MESMA and E(MC)². Results for 25 Monte Carlo runs, brightness normalization, 20 E(MC)² Endmembers, and 100 MESMA models are shown.

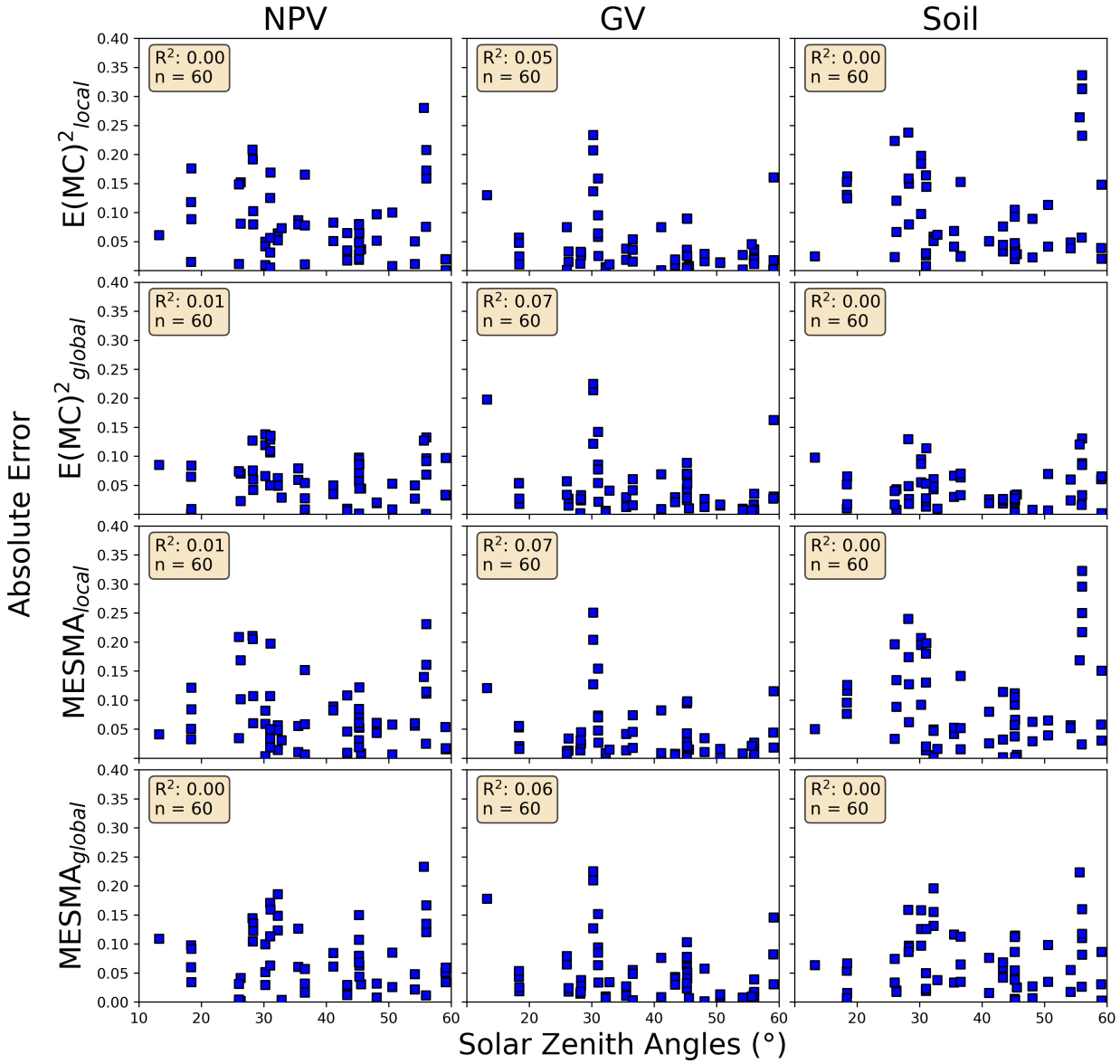

Figure 5: Comparison of NPV, GV, and soil absolute error and solar zenith angles. Results for 25 Monte Carlo runs, brightness normalization, 20 E(MC)² Endmembers, and 100 MESMA models are shown.

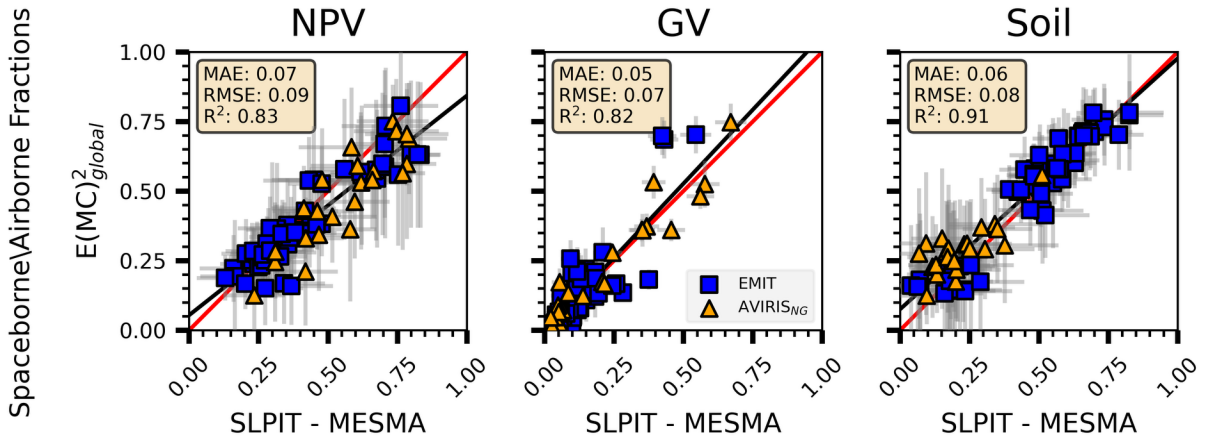

Figure 6: Comparison (n=84) of NPV, GV, and soil estimated fractions from SLPIT using MESMA and Spaceborne/Airborne acquisitions using E(MC)². Retrievals use Monte Carlo runs, brightness normalization, 20 E(MC)² Endmembers, and 100 MESMA models.

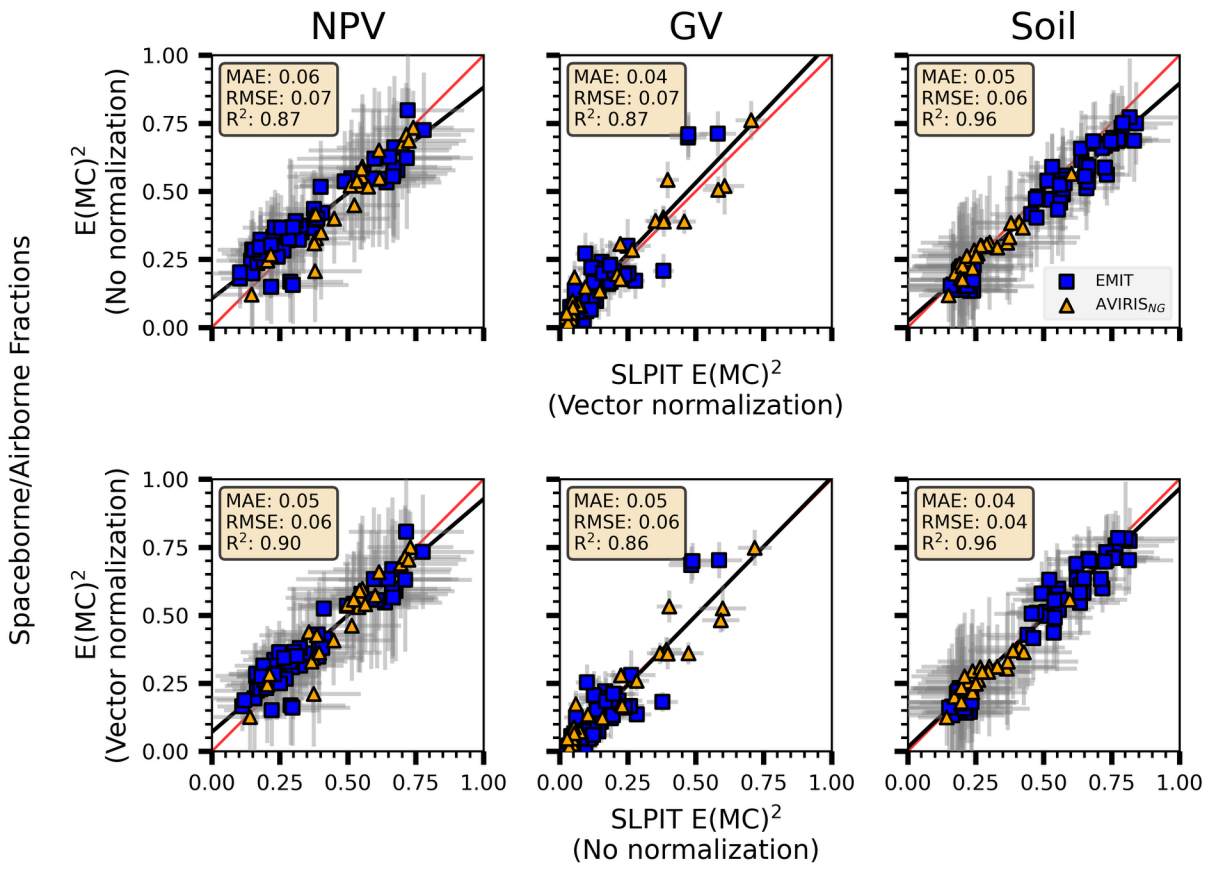

Figure 7: Cross normalization analysis of E(MC)² between SLPIT and image derived fractions (n=84). Results for 25 Monte Carlo runs and 20 E(MC)² Endmembers are shown.

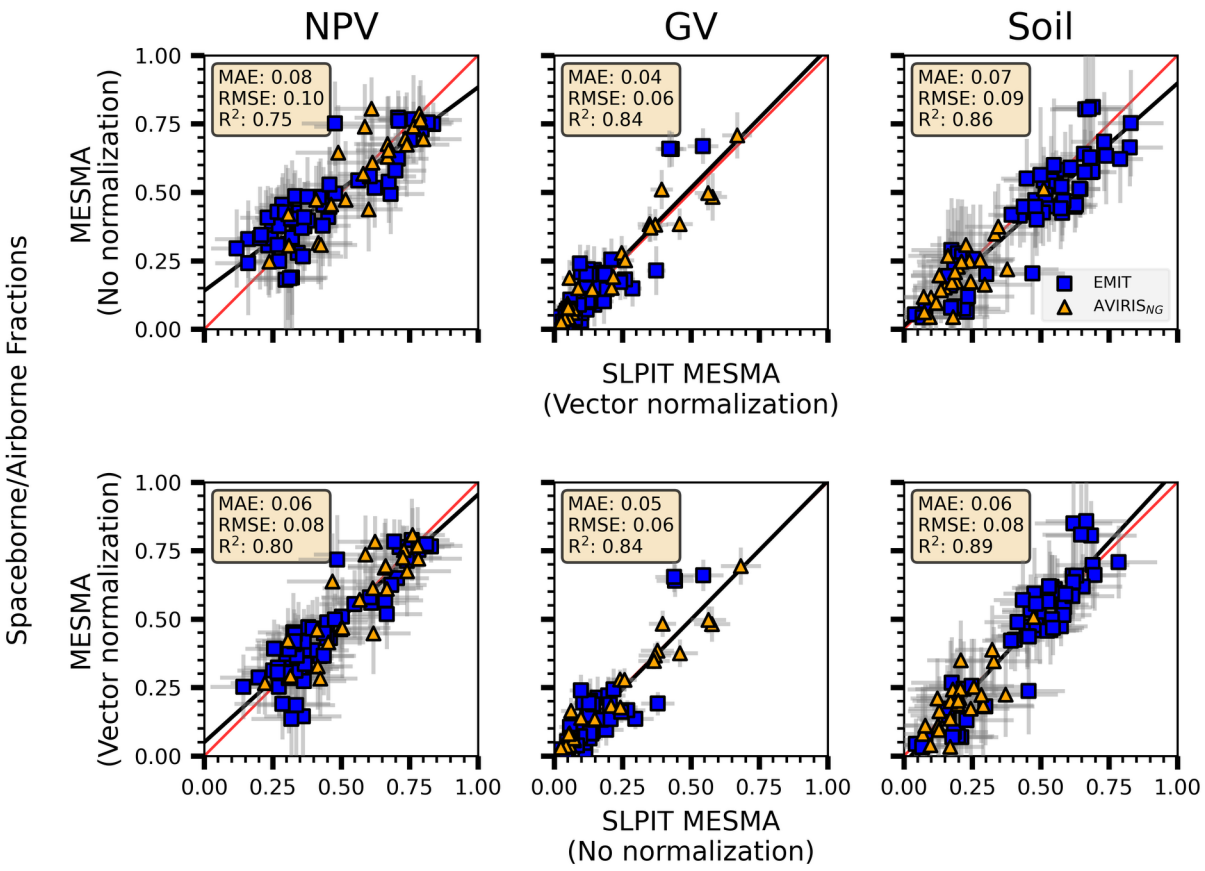

Figure 8: Cross normalization analysis of MESMA between SLPIT and image derived fractions (n=84). Results for 25 Monte Carlo runs and 100 MESMA models are shown.

593

594

595

8. Supplemental

Supplemental Table A: Research sites, names, dates, and coordinates.

Site ID[1]	Sensor	Lat, Long	Site Description	Site Information[2]	Ecoregion	SLPIT Date	EMIT/AVIRIS$_{NG}$ Overpass	Day Difference[3]	Landscape Picture[4]
SPEC - 001	EMIT	35.3748, -116.1116	Shrubland	Koehler et al. (2005)	Mojave	2023-03-11	2023-06-09 t170947	-90	
SPEC - 002	EMIT	35.3743, -116.1105	Shrubland	Koehler et al. (2005)	Mojave	2023-03-11	2023-06-09 t170947	-90	
SPEC - 003	EMIT	32.1915, -113.3387	Playa	Simmons (1966)	Sonoran	2023-03-24	2023-04-15 t222555	-22	
SPEC - 004	EMIT	29.5783, -102.9191	Shrubland	Van Auken and Bush (1992)	Chihuahuan	2023-03-31	2023-03-24 t221318	7	Unavailable
SPEC - 005	EMIT	29.5774, -102.9191	Shrubland	Van Auken and Bush (1992)	Chihuahuan	2023-03-31	2023-03-24 t221318	7	Unavailable
SPEC - 006	EMIT	36.3344, -117.7134	Shrubland	Jesus (2021)	Mojave	2023-04-08	2023-04-05 t190359	3	

SPEC - 007	EMIT	36.3335, -117.7138	Shrubland	Jesus (2021)	Mojave	2023-04-08	2023-04-05 t190359	3	
SPEC - 008	EMIT	36.3338, -117.7122	Shrubland	Jesus (2021)	Mojave	2023-04-08	2023-04-05 t190359	3	
SPEC - 009	EMIT	35.9612, -117.9217	Shrubland	Elmore et al. (2003)	Mojave/ Great Basin	2023-04-15	2023-04-15 t222444	0	
SPEC - 010	EMIT	35.9618, -117.9226	Shrubland	Elmore et al. (2003)	Mojave/ Great Basin	2023-04-15	2023-04-15 t222444	0	
SPEC - 011	EMIT	35.9620, -117.9208	Shrubland	Elmore et al. (2003)	Mojave/ Great Basin	2023-04-15	2023-04-15 t222444	0	

SPEC - 012	EMIT	31.9582, -106.9516	Shrubland	Havstad et al. (2000)	Chihuahuan	2023-04-22	2023-04-16 t213858	6	
SPEC - 013	EMIT	31.9566, -106.9519	Shrubland	Havstad et al. (2000)	Chihuahuan	2023-04-22	2023-04-16 t213858	6	
SPEC - 014	EMIT	34.6927, -120.0343	Grassland	Chadwick et al. (2025)	California Chaparral	2023-04-29	2023-04-26 t182152	3	
SPEC - 015	EMIT	34.6933, -120.0338	Grassland	Chadwick et al. (2025)	California Chaparral	2023-04-29	2023-04-26 t182152	3	
SPEC - 016	EMIT	34.6939, -120.0332	Grassland		California Chaparral	2023-04-29	2023-04-26 t182152	3	

SPEC - 017	EMIT	37.4069, -117.9777	Shrubland	Elmore et al. (2003)	Mojave/ Great Basin	2023-05-12	2023-04-23 t191045	19	
SPEC - 018	EMIT	37.4082, -117.9767	Shrubland	Elmore et al. (2003)	Mojave/ Great Basin	2023-05-12	2023-04-23 t191045	19	
SPEC - 019	EMIT	37.0176, -118.2550	Shrubland	Elmore et al. (2003)	Mojave/ Great Basin	2023-05-13	2023-04-23 t191045	20	
SPEC - 020	EMIT	37.0174, -118.2535	Shrubland	Elmore et al. (2003)	Mojave/ Great Basin	2023-05-13	2023-04-23 t191045	20	
SPEC - 021	EMIT	36.1514, -117.9831	Shrubland	Elmore et al. (2003)	Mojave/ Great Basin	2023-06-03	2023-05-28 t220455	6	

SPEC - 022	EMIT	32.5824, -106.6826	Playa	Havstad et al. (2000)	Chihuahuan	2023-07-12	2023-06-27 t170824	15	
SPEC - 023	EMIT	32.5710, -106.7710	Shrubland	Havstad et al. (2000)	Chihuahuan	2023-07-29	2023-06-27 t170824	32	
SPEC - 024	EMIT	32.5701, -106.7725	Shrubland	Havstad et al. (2000)	Chihuahuan	2023-07-29	2023-06-27 t170824	32	
SPEC - 025	EMIT	32.6503, -106.7586	Shrubland	Havstad et al. (2000)	Chihuahuan	2023-08-03	2023-07-30 t200611	4	
SPEC - 026	EMIT	32.6014, -106.7127	Playa	Havstad et al. (2000)	Chihuahuan	2023-08-03	2023-06-27 t170824	37	

SPEC - 027	EMIT	32.5788, -106.7749	Shrubland	Havstad et al. (2000)	Chihuahuan	2023-08-05	2023-07-30 t200611	6	
SPEC - 028	EMIT	32.5754, -106.7739	Shrubland	Havstad et al. (2000)	Chihuahuan	2023-08-05	2023-07-30 t200611	6	
SPEC - 029	EMIT	32.6932, -106.7824	Shrubland	Havstad et al. (2000)	Chihuahuan	2023-08-10	2023-07-30 t200611	11	
SPEC - 030	EMIT	40.4781, -118.3336	Shrubland	Cohen (1966)	Great Basin	2023-08-22	2023-08-07 t182831	15	
SPEC - 031	EMIT	40.4759, -118.3326	Shrubland	Cohen (1966)	Great Basin	2023-08-22	2023-08-07 t182831	15	

SPEC - 032	EMIT	40.4787, -118.3311	Shrubland	Cohen (1966)	Great Basin	2023-08-23	2023-08-07 t182831	16	
SPEC - 033	EMIT	40.4766, -118.3301	Shrubland	Cohen (1966)	Great Basin	2023-08-23	2023-08-07 t182831	16	
SPEC - 034	EMIT	40.5137, -118.3382	Shrubland	Cohen (1966)	Great Basin	2023-08-24	2023-08-07 t182831	17	
SPEC - 035	EMIT	36.1514, -117.9831	Shrubland	Elmore et al. (2003)	Mojave/ Great Basin	2023-08-25	2023-08-08 t173929	17	
SPEC - 036	EMIT	36.1530, -117.9830	Shrubland	Elmore et al. (2003)	Mojave/ Great Basin	2023-08-25	2023-08-08 t173929	17	

SPEC - 037	EMIT	36.1531, -117.9816	Shrubland	Elmore et al. (2003)	Mojave/ Great Basin	2023-08-25	2023-08-08 t173929	17	
SPEC - 038	EMIT	35.9835, -117.9068	Shrubland	Elmore et al. (2003)	Mojave/ Great Basin	2023-08-26	2023-06-22 t193300	65	
SPEC - 039	EMIT	32.6054, -106.7187	Shrubland	Havstad et al. (2000)	Chihuahuan	2023-09-18	2023-08-31 t152735	18	
SPEC - 040	EMIT	32.5753, -106.7738	Shrubland	Havstad et al. (2000)	Chihuahuan	2023-09-19	2023-08-31 t152735	19	
SPEC - 041	EMIT	32.5702, -106.7727	Shrubland	Havstad et al. (2000)	Chihuahuan	2023-09-19	2023-08-31 t152735	19	

SPEC - 042	EMIT	32.5639, -106.7789	Shrubland	Havstad et al. (2000)	Chihuahuan	2023-09-20	2023-08-31 t152735	20	
SPEC - 043	EMIT	32.5658, -106.7746	Shrubland	Havstad et al. (2000)	Chihuahuan	2023-09-20	2023-08-31 t152735	20	
SPEC - 044	EMIT	32.0103, -106.5180	Shrubland	Havstad et al. (2000)	Chihuahuan	2023-09-22	2023-08-31 t152747	22	
SPEC - 045	EMIT	34.6927, -120.0342	Grassland	Chadwick et al. (2025)	California Chaparral	2023-09-29	2023-09-27 t214531	2	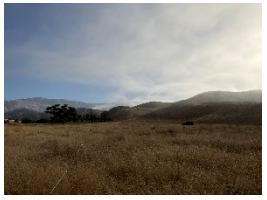
SPEC - 046	EMIT	34.6933, -120.0338	Grassland	Chadwick et al. (2025)	California Chaparral	2023-09-29	2023-09-27 t214531	2	

SPEC - 047	EMIT	34.6939, -120.0332	Grassland	Chadwick et al. (2025)	California Chaparral	2023-09-29	2023-09-27 t214531	2	
SPEC - 048	EMIT	34.6971, -120.0309	Grassland	Chadwick et al. (2025)	California Chaparral	2023-10-04	2023-09-27 t214531	7	
SPEC - 049	EMIT	34.6988, -120.0295	Grassland	Chadwick et al. (2025)	California Chaparral	2023-10-04	2023-09-27 t214531	7	
SPEC - 050	EMIT	34.7402, -120.0279	Grassland	Chadwick et al. (2025)	California Chaparral	2023-10-05	2023-09-27 t214531	8	
SPEC - 051	EMIT	34.7408, -120.0253	Grassland	Chadwick et al. (2025)	California Chaparral	2023-10-06	2023-09-27 t214531	9	

SPEC - 052	EMIT	34.7044, -120.0376	Grassland	Chadwick et al. (2025)	California Chaparral	2023-10-08	2023-09-27 t214531	11	
SPEC - 053	EMIT	34.7000, -120.0378	Grassland	Chadwick et al. (2025)	California Chaparral	2023-10-08	2023-09-27 t214531	11	
SPEC - 054	EMIT	34.6959, -120.0402	Grassland	Chadwick et al. (2025)	California Chaparral	2023-10-10	2023-10-18 t210217	-8	
SPEC - 055	EMIT	34.6895, -120.0392	Grassland	Chadwick et al. (2025)	California Chaparral	2023-10-11	2023-10-18 t210217	-7	
SPEC - 056	EMIT	34.5281, -120.4152	Shrubland	Chadwick et al. (2025)	California Chaparral	2023-10-19	2023-10-14 t224006	5	

SPEC - 057	EMIT	34.4975, -120.4922	Shrubland	Chadwick et al. (2025)	California Chaparral	2023-10-20	2023-10-14 t224006	6	
SPEC - 058	EMIT	34.5211, -120.4586	Grassland	Chadwick et al. (2025)	California Chaparral	2023-10-24	2023-10-14 t224006	10	
SPEC - 059	EMIT	36.7235, -105.6829	Shrubland	Fox et al. (2023)	Chihuahuan	2023-11-14	2023-10-17 t201616	28	
SPEC - 060	EMIT	36.7216, -105.6823	Shrubland	Fox et al. (2023)	Chihuahuan	2023-11-14	2023-10-17 t201616	28	
DPA-004-F	$AVIRIS_{NG}$	34.4985, -120.4907	Shrubland	Chadwick et al. (2025)	California Chaparral	2022-09-17	2022-09-15 t195816	2	

DPB-003-F	AVIRIS$_{NG}$	34.4993, -120.4921	Grassland	Chadwick et al. (2025)	California Chaparral	2022-09-17	2022-09-15 t195816	2	
DPB-004-F	AVIRIS$_{NG}$	34.4972, -120.4912	Grassland	Chadwick et al. (2025)	California Chaparral	2022-09-17	2022-09-15 t200714	2	
DPB-005-F	AVIRIS$_{NG}$	34.4972, -120.4900	Grassland	Chadwick et al. (2025)	California Chaparral	2022-09-17	2022-09-15 t195816	2	
DPB-020-S	AVIRIS$_{NG}$	34.5264, -120.3990	Grassland	Chadwick et al. (2025)	California Chaparral	2022-03-24	2022-03-22 t204749	2	
DPB-027-S	AVIRIS$_{NG}$	34.5375, -120.4578	Shrubland	Chadwick et al. (2025)	California Chaparral	2022-04-14	2022-04-12 t205405	2	

SRA-007-F	AVIRIS$_{NG}$	34.6929, -120.0339	Grassland	Chadwick et al. (2025)	California Chaparral	2022-09-16	2022-09-14 t184300	2	
SRA-008-F	AVIRIS$_{NG}$	34.7430, -119.9851	Shrubland	Chadwick et al. (2025)	California Chaparral	2022-09-16	2022-09-14 t184300	2	
SRA-019-S	AVIRIS$_{NG}$	34.7428, -119.9847	Grassland	Chadwick et al. (2025)	California Chaparral	2022-03-10	2022-03-08 t204043	2	
SRA-020-S	AVIRIS$_{NG}$	34.7029, -120.0414	Grassland	Chadwick et al. (2025)	California Chaparral	2022-03-10	2022-03-08 t205512	2	
SRA-021-S	AVIRIS$_{NG}$	34.7033, -120.0423	Grassland	Chadwick et al. (2025)	California Chaparral	2022-03-10	2022-03-08 t204043	2	

SRA-033-S	AVIRIS$_{NG}$	34.7049, -120.0383	Grassland	Chadwick et al. (2025)	California Chaparral	2022-03-18	2022-03-16 t210303	2	
SRA-034-S	AVIRIS$_{NG}$	34.6866, -120.0340	Grassland	Chadwick et al. (2025)	California Chaparral	2022-03-18	2022-03-16 t210303	2	
SRA-056-F	AVIRIS$_{NG}$	34.6867, -120.0349	Grassland	Chadwick et al. (2025)	California Chaparral	2022-09-16	2022-09-14 t184300	2	
SRA-109-S	AVIRIS$_{NG}$	34.7419, -119.9855	Grassland	Chadwick et al. (2025)	California Chaparral	2022-05-13	2022-05-11 t190344	2	
SRB-010-F	AVIRIS$_{NG}$	34.7054, -120.0379	Grassland	Chadwick et al. (2025)	California Chaparral	2022-09-15	2022-09-15 t203517	0	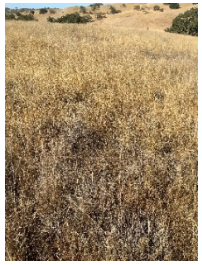

SRB-021-S	$AVIRIS_{NG}$	34.7424, -119.9840	Grassland	Chadwick et al. (2025)	California Chaparral	2022-03-10	2022-03-08 t205512	2	
SRB-026-S	$AVIRIS_{NG}$	34.6990, -120.0373	Shrubland	Chadwick et al. (2025)	California Chaparral	2022-03-11	2022-03-08 t204043	3	
SRB-045-F	$AVIRIS_{NG}$	34.7034, -120.0416	Grassland	Chadwick et al. (2025)	California Chaparral	2022-09-15	2022-09-15 t203517	0	
SRB-046-F	$AVIRIS_{NG}$	34.6924, -120.0510	Grassland	Chadwick et al. (2025)	California Chaparral	2022-09-15	2022-09-15 t203517	0	
SRB-047-S	$AVIRIS_{NG}$	34.6993, -120.0382	Grassland	Chadwick et al. (2025)	California Chaparral	2022-04-07	2022-04-05 t201359	2	

SRB-050-F	$AVIRIS_{NG}$	34.7419, -119.9860	Grassland	Chadwick et al. (2025)	California Chaparral	2022-09-16	2022-09-14 t184300	2	
SRB-084-S	$AVIRIS_{NG}$	34.7001, -120.0369	Grassland	Chadwick et al. (2025)	California Chaparral	2022-05-13	2022-05-11 t191813	2	
SRB-100-F	$AVIRIS_{NG}$	34.6997, -120.0369	Grassland	Chadwick et al. 2025	California Chaparral	2022-09-15	2022-09-15 t203517	0	

[1]F indicates Fall portion of SHIFT campaign, S indicates Spring portion of SHIFT 2022 campaign.
[2]Information about site climate and vegetation could be found in these studies.
[3]Positive values indicate days after overpass when SLPIT sampling occurred, negative values indicate days before overpass when SLPIT sampling occurred.
[4]Landscpace pictures for AVIRISNG sites were sourced from Queally et al. 2024.

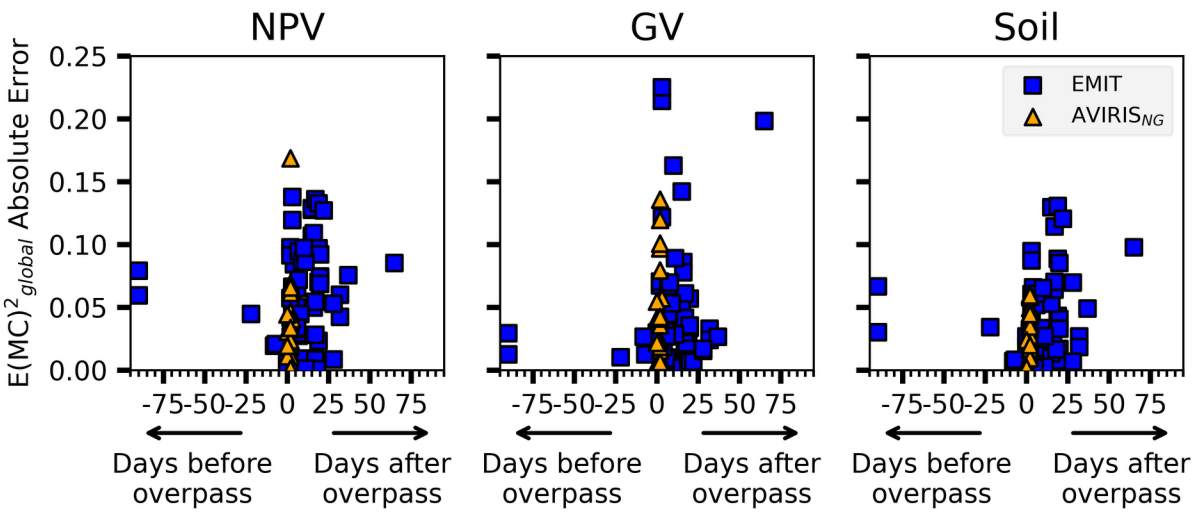

Supplemental Figure A: Distribution of fractional cover unmixing error as function of time between SLPIT field sampling and associated EMIT or AVIRIS$_{NG}$ acquisition.

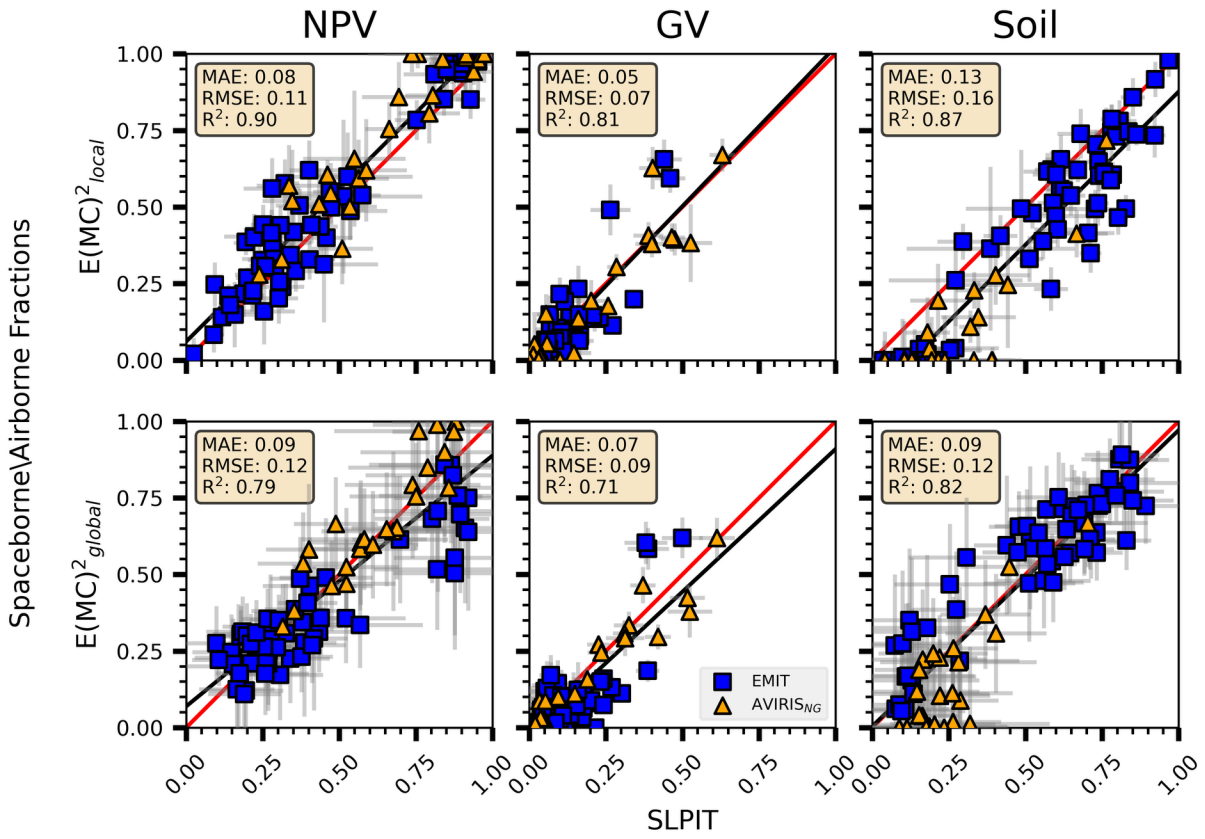

Supplemental Figure B: Comparison of NPV, GV, and soil estimated fractions from SLPIT and EMIT using E(MC)² (n=84). Results for the "best" solution (e.g., lowest spectral error) of the 25 Monte Carlo runs, brightness normalization, 20 E(MC)² endmembers are shown.

620

621

9. References

Adams, J.B., Smith, M.O., Johnson, P.E., 1986. Spectral mixture modeling: A new analysis of rock and soil types at the Viking Lander 1 Site. Journal of Geophysical Research: Solid Earth 91, 8098–8112. https://doi.org/10.1029/JB091iB08p08098

Amundson, R., Ewing, S., Dietrich, W., Sutter, B., Owen, J., Chadwick, O., Nishiizumi, K., Walvoord, M., McKay, C., 2008. On the *in situ* aqueous alteration of soils on Mars. Geochimica et Cosmochimica Acta 72, 3845–3864. https://doi.org/10.1016/j.gca.2008.04.038

Angel, Y., Raiho, A., Kathuria, D., Chadwick, K.D., Brodrick, P.G., Lang, E., Ochoa, F., Shiklomanov, A.N., 2025. Deciphering the spectra of flowers to map landscape-scale blooming dynamics. Ecosphere 16, e70127. https://doi.org/10.1002/ecs2.70127

Asner, G.P., Heidebrecht, K.B., 2002. Spectral unmixing of vegetation, soil and dry carbon cover in arid regions: Comparing multispectral and hyperspectral observations. International Journal of Remote Sensing 23, 3939–3958. https://doi.org/10.1080/01431160110115960

Asner, G.P., Wessman, C.A., Bateson, C.A., Privette, J.L., 2000. Impact of Tissue, Canopy, and Landscape Factors on the Hyperspectral Reflectance Variability of Arid Ecosystems. Remote Sensing of Environment 74, 69–84. https://doi.org/10.1016/S0034-4257(00)00124-3

Brodrick, P.G., Chlus, A.M., Pavlick, R., Bernas, M., Chapman, J.W., Eckert, R., Helmlinger, M., Hess-Flores, M., Rios, L.M., Schneider, F.D., Smyth, M.M., Eastwood, M., Green, R.O., Thompson, D.R., Chadwick, K.D., Schimel, D.S., 2025a. SBG High Frequency Time Series (SHIFT)SHIFT: AVIRIS-NG L2A Orthorectified Surface Reflectance, V2. https://doi.org/10.3334/ORNLDAAC/2431

Brodrick, P.G., Isofit, Erickson, A., Winstonolson, Thompson, D.R., Jfahlen, Shiklomanov, A., Serbin, S.P., NimrodCarmon, Yshinozu, McGibbney, L.J., Unbohn, 2022. isofit/isofit: 2.9.3. https://doi.org/10.5281/ZENODO.6908949

Brodrick, P.G., Ochoa, F., Okin, G., Jhalani, V.A., Olson-Duvall, W., Lundeen, S.R., Thompson, D.R., Green, R.O., 2025b. SpectralUnmixing: A general Julia package for unmixing spectroscopy data. JOSS 10, 9149. https://doi.org/10.21105/joss.09149

Chadwick, K.D., Davis, F., Miner, K.R., Pavlick, R., Reynolds, M., Townsend, P.A., Brodrick, P.G., Ade, C., Allen, J., Anderegg, L., Angel, Y., Boving, I., Byrd, K.B., Campbell, P., Carberry, L., Cavanaugh, Katherine C., Cavanaugh, Kyle C., Easterday, K., Eckert, R., Gierach, M., Gold, K., Hestir, E., Huemmrich, F., Klope, M., Kokaly, R.F., Lovegreen, P., Luis, K., McMahon, C., Nidzieko, N., Ochoa, F., Ongjoco, A.J., Ordway, E., Pascolini-Campbell, M., Queally, N., Roberts, D.A., Saiki, C.M., Schneider, F.D., Shiklomanov, A.N., Silva, G.D., Snyder, J., Thornton, M., Trugman, A.T., Vinod, N., Zheng, T., Avouris, D.M., Baker, B., Baskaran, L., Bell, T., Berg, M., Bernas, M., Bohn, N., Braghiere, R.K., Breuer, Z., Brooks, A.J., Burkard, N., Burmistrova, J., Cawse-Nicholson, K., Chapman, J., Chazaro-Haraksin, J., Cryer, J., Cushman, K.C., Dahlin, K., Dao, P.D., DiBartolo, A., Eastwood, M., Elder, C.D., Giordani, A., Grant, K., Green, R.O., Hanson, A., Heberlein, B., Helmlinger, M., Hook, S., Jensen, D., Johnson, E., Johnson, M., Kiper, M., Kibler, C., King, J.Y., Kovach, K.R., Kreisberg, A., Lacey, D., Lang, E., Lee, C., Lopez, A.M., Lopez Barreto, B., Maguire, A., Marsh, E., Miller, C., Nguyen, D.M.T., Nickles, C., Ocón, J.P., Papen, E.P., Park, M., Poulter, B., Raiho, A., Reim, P., Robinson, T.H., Romero Galvan, F.E., Shafron, E., Skalitzky, B.R.,

Stroschein, S., Taylor, N.C., Thompson, D.R., Thompson, K., Tye, C., Van Beek, J., Vanden Heuvel, C., Vellanoweth, J., Vermeer, E., Villanueva-Weeks, C., Zumdahl, K., Schimel, D., 2025. Unlocking ecological insights from sub-seasonal visible-to-shortwave infrared imaging spectroscopy: The SHIFT campaign. Ecosphere 16, e70194. https://doi.org/10.1002/ecs2.70194

Chapman, J.W., Thompson, D.R., Helmlinger, M.C., Bue, B.D., Green, R.O., Eastwood, M.L., Geier, S., Olson-Duvall, W., Lundeen, S.R., 2019. Spectral and Radiometric Calibration of the Next Generation Airborne Visible Infrared Spectrometer (AVIRIS-NG). Remote Sensing 11, 2129. https://doi.org/10.3390/rs11182129

Clark, R.N., Swayze, G.A., Brodrick, P.G., Green, R.O., Mahowald, N.M., Thompson, D.R., Ehlmann, B.L., Ginoux, P.A., Kalashnikova, O.V., Keebler, A., 2022. Minerals and Other Materials Identification and Mapping with EMIT. Presented at the AGU Fall Meeting Abstracts, pp. GC35A-02.

Clark, R.N., Swayze, G.A., Livo, K.E., Kokaly, R.F., Sutley, S.J., Dalton, J.B., McDougal, R.R., Gent, C.A., 2003. Imaging spectroscopy: Earth and planetary remote sensing with the USGS Tetracorder and expert systems. Journal of Geophysical Research: Planets 108. https://doi.org/10.1029/2002JE001847

Cohen, P., 1966. Water in the Humboldt River Valley near Winnemucca, Nevada. https://doi.org/10.3133/wsp1816

Coleman, R.W., Thompson, D.R., Brodrick, P.G., Dor, E.B., Cox, E., García-Pando, C.P., Hoefen, T., Kokaly, R.F., Meyer, J.M., Ochoa, F., 2024. An accuracy assessment of the surface reflectance product from the EMIT imaging spectrometer. Remote Sensing of Environment 315, 114450.

Curran, P.J., 1989. Remote sensing of foliar chemistry. Remote Sensing of Environment 30, 271–278. https://doi.org/10.1016/0034-4257(89)90069-2

Czekajlo, A., Coops, N.C., Goodbody, T.R.H., 2021. Untangling the effect of urban vegetation type and structure on spectrally unmixed greenness. Remote Sensing Letters 12, 1216–1226. https://doi.org/10.1080/2150704X.2021.1978580

Daughtry, C.S.T., Hunt, E.R., 2008. Mitigating the effects of soil and residue water contents on remotely sensed estimates of crop residue cover. Remote Sensing of Environment, Remote Sensing Data Assimilation Special Issue 112, 1647–1657. https://doi.org/10.1016/j.rse.2007.08.006

Dennison, P.E., Halligan, K.Q., Roberts, D.A., 2004. A comparison of error metrics and constraints for multiple endmember spectral mixture analysis and spectral angle mapper. Remote Sensing of Environment 93, 359–367. https://doi.org/10.1016/j.rse.2004.07.013

Dennison, P.E., Lamb, B.T., Campbell, M.J., Kokaly, R.F., Hively, W.D., Vermote, E., Dabney, P., Serbin, G., Quemada, M., Daughtry, C.S.T., Masek, J., Wu, Z., 2023. Modeling global indices for estimating non-photosynthetic vegetation cover. Remote Sensing of Environment 295, 113715. https://doi.org/10.1016/j.rse.2023.113715

Dennison, P.E., Qi, Y., Meerdink, S.K., Kokaly, R.F., Thompson, D.R., Daughtry, C.S.T., Quemada, M., Roberts, D.A., Gader, P.D., Wetherley, E.B., Numata, I., Roth, K.L., 2019. Comparison of Methods for Modeling Fractional Cover Using Simulated Satellite Hyperspectral Imager Spectra. Remote Sensing 11, 2072. https://doi.org/10.3390/rs11182072

711 Dennison, P.E., Roberts, D.A., 2003. Endmember selection for multiple endmember spectral
712 mixture analysis using endmember average RMSE. Remote Sensing of Environment
713 87, 123–135. https://doi.org/10.1016/S0034-4257(03)00135-4
714 Elmore, A.J., Mustard, J.F., Manning, S.J., 2003. Regional Patterns of Plant Community
715 Response to Changes in Water: Owens Valley, California. Ecological Applications 13,
716 443–460. https://doi.org/10.1890/1051-
717 0761(2003)013%255B0443:RPOPCR%255D2.0.CO;2
718 Fisk, C., Clarke, K., Delean, S., Lewis, M., 2019a. Distinguishing Photosynthetic and Non-
719 Photosynthetic Vegetation: How Do Traditional Observations and Spectral
720 Classification Compare? Remote Sensing 11, 2589.
721 https://doi.org/10.3390/rs11212589
722 Fisk, C., Clarke, K., Lewis, M., 2019b. Comparison of Hyperspectral Versus Traditional Field
723 Measurements of Fractional Ground Cover in the Australian Arid Zone. Remote
724 Sensing 11, 2825. https://doi.org/10.3390/rs11232825
725 Fox, K.M., Margolis, E.Q., Lopez, M.K., Kasten, E.A., Stevens, J.T., 2023. Vegetation change over
726 140 years in a sagebrush landscape of the Rio Grande del Norte National Monument,
727 New Mexico, USA. Journal of Vegetation Science 34, e13202.
728 https://doi.org/10.1111/jvs.13202
729 Gill, T.K., Phinn, S.R., 2009. Improvements to ASTER-Derived Fractional Estimates of Bare
730 Ground in a Savanna Rangeland. IEEE Transactions on Geoscience and Remote
731 Sensing 47, 662–670. https://doi.org/10.1109/TGRS.2008.2004628
732 Gill, T.K., Phinn, S.R., 2008. Estimates of bare ground and vegetation cover from Advanced
733 Spaceborne Thermal Emission and Reflection Radiometer (ASTER) short-wave-
734 infrared reflectance imagery. JARS 2, 023511. https://doi.org/10.1117/1.2907748
735 Gitelson, A., Merzlyak, M.N., 1994. Spectral Reflectance Changes Associated with Autumn
736 Senescence of Aesculus hippocastanum L. and Acer platanoides L. Leaves. Spectral
737 Features and Relation to Chlorophyll Estimation. Journal of Plant Physiology 143,
738 286–292. https://doi.org/10.1016/S0176-1617(11)81633-0
739 Green, R.O., 2022. EMIT L2A Estimated Surface Reflectance and Uncertainty and Masks 60 m
740 V001. https://doi.org/10.5067/EMIT/EMITL2ARFL.001
741 Green, R.O., Mahowald, N., Ung, C., Thompson, D.R., Bator, L., Bennet, M., Bernas, M.,
742 Blackway, N., Bradley, C., Cha, J., Clark, P., Clark, R., Cloud, D., Diaz, E., Ben Dor, E.,
743 Duren, R., Eastwood, M., Ehlmann, B.L., Fuentes, L., Ginoux, P., Gross, J., He, Y.,
744 Kalashnikova, O., Kert, W., Keymeulen, D., Klimesh, M., Ku, D., Kwong-Fu, H., Liggett,
745 E., Li, L., Lundeen, S., Makowski, M.D., Mazer, A., Miller, R., Mouroulis, P., Oaida, B.,
746 Okin, G.S., Ortega, A., Oyake, A., Nguyen, H., Pace, T., Painter, T.H., Pempejian, J., Garcia-
747 Pando, C.P., Pham, T., Phillips, B., Pollock, R., Purcell, R., Realmuto, V., Schoolcraft, J.,
748 Sen, A., Shin, S., Shaw, L., Soriano, M., Swayze, G., Thingvold, E., Vaid, A., Zan, J., 2020.
749 The Earth Surface Mineral Dust Source Investigation: An Earth Science Imaging
750 Spectroscopy Mission, in: 2020 IEEE Aerospace Conference. Presented at the 2020
751 IEEE Aerospace Conference, pp. 1–15.
752 https://doi.org/10.1109/AERO47225.2020.9172731
753 Green, R.O., Sen, A., Pearson, J.C., Mouroulis, P., Patel, S., Sullivan, P., Werne, T., Brenner, M.,
754 McKinley, I., Liggett, E., Rodriguez, J., Eastwood, M., Smith, Susan.T., Diaz, E., Bennett,
755 M., Pollock, R., Walch, M., 2022. Surface Biology and Geology (SBG) Visible to Short
756 Wavelength Infrared (VSWIR) Wide Swath Instrument Concept, in: 2022 IEEE

Aerospace Conference (AERO). Presented at the 2022 IEEE Aerospace Conference (AERO), pp. 1–10. https://doi.org/10.1109/AERO53065.2022.9843676

Guerschman, J.P., Hill, M.J., 2018. Calibration and validation of the Australian fractional cover product for MODIS collection 6. Remote Sensing Letters 9, 696–705. https://doi.org/10.1080/2150704X.2018.1465611

Guerschman, J.P., Hill, M.J., Renzullo, L.J., Barrett, D.J., Marks, A.S., Botha, E.J., 2009. Estimating fractional cover of photosynthetic vegetation, non-photosynthetic vegetation and bare soil in the Australian tropical savanna region upscaling the EO-1 Hyperion and MODIS sensors. Remote Sensing of Environment 113, 928–945. https://doi.org/10.1016/j.rse.2009.01.006

Guerschman, J.P., Oyarzabal, M., Malthus, T., McVicar, T., Byrne, G., Randall, L., Stewart, J., 2012. Evaluation of the MODIS-based vegetation fractional cover product.

Guerschman, J.P., Scarth, P.F., McVicar, T.R., Renzullo, L.J., Malthus, T.J., Stewart, J.B., Rickards, J.E., Trevithick, R., 2015. Assessing the effects of site heterogeneity and soil properties when unmixing photosynthetic vegetation, non-photosynthetic vegetation and bare soil fractions from Landsat and MODIS data. Remote Sensing of Environment 161, 12–26. https://doi.org/10.1016/j.rse.2015.01.021

Havstad, K.M., Kustas, W.P., Rango, A., Ritchie, J.C., Schmugge, T.J., 2000. Jornada Experimental Range: A Unique Arid Land Location for Experiments to Validate Satellite Systems. Remote Sensing of Environment 74, 13–25. https://doi.org/10.1016/S0034-4257(00)00118-8

Jesus, M., 2021. A Vascular Flora of the Southern Inyo Mountains, Inyo County, California (M.S.). ProQuest Dissertations and Theses. The Claremont Graduate University, United States -- California.

Koehler, P.A., Anderson, R.S., Spaulding, W.G., 2005. Development of vegetation in the Central Mojave Desert of California during the late Quaternary. Palaeogeography, Palaeoclimatology, Palaeoecology 215, 297–311. https://doi.org/10.1016/j.palaeo.2004.09.010

Kokaly, R.F., Clark, R.N., Swayze, G.A., Livo, K.E., Hoefen, T.M., Pearson, N.C., Wise, R.A., Benzel, W.M., Lowers, H.A., Driscoll, R.L., Klein, A.J., 2017. USGS Spectral Library Version 7 Data. https://doi.org/10.5066/F7RR1WDJ

Kokaly, R.F., Skidmore, A.K., 2015. Plant phenolics and absorption features in vegetation reflectance spectra near 1.66 μm. International Journal of Applied Earth Observation and Geoinformation 43, 55–83. https://doi.org/10.1016/j.jag.2015.01.010

Liu, D., Jia, K., Wei, X., Xia, M., Zhang, Xiwang, Yao, Y., Zhang, Xiaotong, Wang, B., 2019. Spatiotemporal Comparison and Validation of Three Global-Scale Fractional Vegetation Cover Products. Remote Sensing 11, 2524. https://doi.org/10.3390/rs11212524

Meyer, T., Okin, G.S., 2015. Evaluation of spectral unmixing techniques using MODIS in a structurally complex savanna environment for retrieval of green vegetation, nonphotosynthetic vegetation, and soil fractional cover. Remote Sensing of Environment 161, 122–130. https://doi.org/10.1016/j.rse.2015.02.013

Mu, X., Hu, M., Song, W., Ruan, G., Ge, Y., Wang, J., Huang, S., Yan, G., 2015. Evaluation of Sampling Methods for Validation of Remotely Sensed Fractional Vegetation Cover. Remote Sensing 7, 16164–16182. https://doi.org/10.3390/rs71215817

Muir, J., Schmidt, M., Tindall, D., Trevithick, R., Scarth, P., Stewart, J., 2011. Field measurement of fractional ground cover: a technical handbook supporting ground cover monitoring for Australia. Australian Bureau of Agricultural and Resource Economics and Sciences (ABARES): Canberra, Australia.

Nieke, J., Despoisse, L., Gabriele, A., Weber, H., Strese, H., Ghasemi, N., Gascon, F., Alonso, K., Boccia, V., Tsonevska, B., Choukroun, P., Ottavianelli, G., Celesti, M., 2023. The copernicus hyperspectral imaging mission for the environment (CHIME): an overview of its mission, system and planning status, in: Sensors, Systems, and Next-Generation Satellites XXVII. Presented at the Sensors, Systems, and Next-Generation Satellites XXVII, SPIE, pp. 21–40. https://doi.org/10.1117/12.2679977

Numata, I., Roberts, D.A., Chadwick, O.A., Schimel, J.P., Galvão, L.S., Soares, J.V., 2008. Evaluation of hyperspectral data for pasture estimate in the Brazilian Amazon using field and imaging spectrometers. Remote Sensing of Environment, Remote Sensing Data Assimilation Special Issue 112, 1569–1583. https://doi.org/10.1016/j.rse.2007.08.014

Ochoa, F., Brodrick, P., Ochoa Gonzalez, J.A., LeGrand, S.L., Gillespie, M.N., Coleman, R.W., Ade, C., Alley, K., Kerches Braghiere, R., Angel, Y., Chadwick, K.D., Daley, J., Delucchi, C., Eckert, R.F., Gallegos, A., Grant, K., Green, R.O., Davis, F., Dao, P.D., Kiebler, C., Kreisber, A., Maguire, A., Meyer, T., Newhouse, M., Quintero, J., Roberts, D.A., Schneider, F., Thompson, D.R., Thompson, K., Shortridge, F., Sonobe, D., Zumdahl, K., Okin, G.S., 2026. SLPIT in support of fractional cover validation. https://doi.org/10.5281/ZENODO.18971595

Ochoa, F., Brodrick, P., Okin, G., 2025a. terraspec. https://doi.org/10.5281/ZENODO.14867412

Ochoa, F., Brodrick, P.G., Okin, G.S., Ben-Dor, E., Meyer, T., Thompson, D.R., Green, R.O., 2025b. Soil and vegetation cover estimation for global imaging spectroscopy using spectral mixture analysis. Remote Sensing of Environment 324, 114746. https://doi.org/10.1016/j.rse.2025.114746

Ochoa, F., Brodrick, P.G., Okin, G.S., Chadwick, K.D., Thompson, D.R., Green, R.O., LeGrand, S., Ochoa-Gonzalez, J.A., Angel, Y., Rahio, A., Braghiere, R.K., Eckert, R., Schneider, F.D., Kreisberg, A., Thompson, K., Dao, P., Davis, F., 2024. Drylands spectral libraries in support of EMIT. https://doi.org/10.21232/QIJXNPFT

Okin, G.S., 2007. Relative spectral mixture analysis — A multitemporal index of total vegetation cover. Remote Sensing of Environment 106, 467–479. https://doi.org/10.1016/j.rse.2006.09.018

Okin, G.S., Clarke, K.D., Lewis, M.M., 2013. Comparison of methods for estimation of absolute vegetation and soil fractional cover using MODIS normalized BRDF-adjusted reflectance data. Remote Sensing of Environment 130, 266–279. https://doi.org/10.1016/j.rse.2012.11.021

Okin, G.S., Roberts, D.A., Murray, B., Okin, W.J., 2001. Practical limits on hyperspectral vegetation discrimination in arid and semiarid environments. Remote Sensing of Environment 77, 212–225. https://doi.org/10.1016/S0034-4257(01)00207-3

Queally, N., Davis, F.W., Chadwick, K.D., Ade, C., Anderegg, L., Angel, Y., Baker, B., Baskaran, L., Boving, I., Braghiere, R.K., 2024. SHIFT: Vegetation Plot Photos, Santa Barbara, CA, USA, 2022. ORNL DAAC, Oak Ridge, Tennessee, USA.

Ray, T.W., Murray, B.C., 1996. Nonlinear spectral mixing in desert vegetation. Remote Sensing of Environment 55, 59–64. https://doi.org/10.1016/0034-4257(95)00171-9

Rigge, M., Homer, C., Shi, H., K. Meyer, D., 2019. Validating a Landsat Time-Series of Fractional Component Cover Across Western U.S. Rangelands. Remote Sensing 11, 3009. https://doi.org/10.3390/rs11243009

Roberts, D.A., Gardner, M., Church, R., Ustin, S., Scheer, G., Green, R.O., 1998. Mapping Chaparral in the Santa Monica Mountains Using Multiple Endmember Spectral Mixture Models. Remote Sensing of Environment 65, 267–279. https://doi.org/10.1016/S0034-4257(98)00037-6

Roberts, D.A., Smith, M.O., Adams, J.B., 1993. Green vegetation, nonphotosynthetic vegetation, and soils in AVIRIS data. Remote Sensing of Environment, Airbone Imaging Spectrometry 44, 255–269. https://doi.org/10.1016/0034-4257(93)90020-X

Scarth, P., Guerschman, J.P., Clarke, K., Phinn, S., 2015. Validation of Australian fractional cover products from MODIS and Landsat data. AusCover good practice guidelines: a technical handbook supporting calibration and validation activities of remotely sensed data Product 123–138.

Schug, F., Frantz, D., Okujeni, A., van der Linden, S., Hostert, P., 2020. Mapping urban-rural gradients of settlements and vegetation at national scale using Sentinel-2 spectral-temporal metrics and regression-based unmixing with synthetic training data. Remote Sensing of Environment 246, 111810. https://doi.org/10.1016/j.rse.2020.111810

Schug, F., Okujeni, A., Hauer, J., Hostert, P., Nielsen, J.Ø., van der Linden, S., 2018. Mapping patterns of urban development in Ouagadougou, Burkina Faso, using machine learning regression modeling with bi-seasonal Landsat time series. Remote Sensing of Environment 210, 217–228. https://doi.org/10.1016/j.rse.2018.03.022

Senf, C., Laštovička, J., Okujeni, A., Heurich, M., van der Linden, S., 2020. A generalized regression-based unmixing model for mapping forest cover fractions throughout three decades of Landsat data. Remote Sensing of Environment 240, 111691. https://doi.org/10.1016/j.rse.2020.111691

Shimabukuro, Y.E., Smith, J.A., 1991. The least-squares mixing models to generate fraction images derived from remote sensing multispectral data. IEEE Transactions on Geoscience and Remote Sensing 29, 16–20. https://doi.org/10.1109/36.103288

Simmons, N.M., 1966. Flora of the Cabeza Prieta Game Range. Journal of the Arizona Academy of Science 4, 93–104. https://doi.org/10.2307/40022377

Stavros, E.N., Chrone, J., Cawse-Nicholson, K., Freeman, A., Glenn, N.F., Guild, L., Kokaly, R., Lee, C., Luvall, J., Pavlick, R., Poulter, B., Schollaert Uz, S., Serbin, S., Thompson, D.R., Townsend, P.A., Turpie, K., Yuen, K., Thome, K., Wang, W., Zareh, S., Nastal, J., Bearden, D., Miller, C.E., Schimel, D., 2023. Designing an Observing System to Study the Surface Biology and Geology (SBG) of the Earth in the 2020s. JGR Biogeosciences 128, e2021JG006471. https://doi.org/10.1029/2021JG006471

Sutton, A., Fisher, A., Metternicht, G., 2022. Assessing the Accuracy of Landsat Vegetation Fractional Cover for Monitoring Australian Drylands. Remote Sensing 14, 6322. https://doi.org/10.3390/rs14246322

Thompson, D.R., Green, R.O., Bradley, C., Brodrick, P.G., Mahowald, N., Dor, E.B., Bennett, M., Bernas, M., Carmon, N., Chadwick, K.D., Clark, R.N., Coleman, R.W., Cox, E., Diaz, E., Eastwood, M.L., Eckert, R., Ehlmann, B.L., Ginoux, P., Ageitos, M.G., Grant, K., Guanter, L., Pearlshtien, D.H., Helmlinger, M., Herzog, H., Hoefen, T., Huang, Y., Keebler, A., Kalashnikova, O., Keymeulen, D., Kokaly, R., Klose, M., Li, L., Lundeen, S.R., Meyer, J., Middleton, E., Miller, R.L., Mouroulis, P., Oaida, B., Obiso, V., Ochoa, F., Olson-Duvall, W., Okin, G.S., Painter, T.H., Pérez García-Pando, C., Pollock, R., Realmuto, V., Shaw, L., Sullivan, P., Swayze, G., Thingvold, E., Thorpe, A.K., Vannan, S., Villarreal, C., Ung, C., Wilson, D.W., Zandbergen, S., 2024. On-orbit calibration and performance of the EMIT imaging spectrometer. Remote Sensing of Environment 303, 113986. https://doi.org/10.1016/j.rse.2023.113986

Thompson, D.R., Natraj, V., Green, R.O., Helmlinger, M.C., Gao, B.-C., Eastwood, M.L., 2018. Optimal estimation for imaging spectrometer atmospheric correction. Remote Sensing of Environment 216, 355–373. https://doi.org/10.1016/j.rse.2018.07.003

Thompson, D.R., Schimel, D.S., Poulter, B., Brosnan, I., Hook, S.J., Green, R.O., Glenn, N., Guild, L., Henn, C., Cawse-Nicholson, K., Kokaly, R., Lee, C., Luvall, J., Miller, C.E., Nastal, J., Pavlick, R., Phillips, B., Schneider, F., Uz, S.S., Serbin, S., Stavros, N., Townsend, P., Turner, W., Turpie, K., Wang, W., 2020. NASA's Surface Biology and Geology Concept Study: Status and Next Steps, in: IGARSS 2020 - 2020 IEEE International Geoscience and Remote Sensing Symposium. Presented at the IGARSS 2020 - 2020 IEEE International Geoscience and Remote Sensing Symposium, IEEE, Waikoloa, HI, USA, pp. 3269–3271. https://doi.org/10.1109/IGARSS39084.2020.9323295

Thorpe, A.K., Green, R.O., Thompson, D.R., Brodrick, P.G., Chapman, J.W., Elder, C.D., Irakulis-Loitxate, I., Cusworth, D.H., Ayasse, A.K., Duren, R.M., Frankenberg, C., Guanter, L., Worden, J.R., Dennison, P.E., Roberts, D.A., Chadwick, K.D., Eastwood, M.L., Fahlen, J.E., Miller, C.E., 2023. Attribution of individual methane and carbon dioxide emission sources using EMIT observations from space. Science Advances 9, eadh2391. https://doi.org/10.1126/sciadv.adh2391

Townshend, J.R.G., Huang, C., Kalluri, S.N.V., Defries, R.S., Liang, S., Yang, K., 2000. Beware of per-pixel characterization of land cover. International Journal of Remote Sensing 21, 839–843. https://doi.org/10.1080/014311600210641

Trevithick, R., Muir, J., Denham, R., 2012. The effect of observer experience levels on the variability of fractional ground cover reference data. Proceeding of the 16th Annual ARSPC, Melbourne, Australia, August.

Tsendbazar, N.-E., Herold, M., de Bruin, S., Lesiv, M., Fritz, S., Van De Kerchove, R., Buchhorn, M., Duerauer, M., Szantoi, Z., Pekel, J.-F., 2018. Developing and applying a multi-purpose land cover validation dataset for Africa. Remote Sensing of Environment 219, 298–309. https://doi.org/10.1016/j.rse.2018.10.025

Van Auken, O.W., Bush, J.K., 1992. Factors Influencing the Density and Distribution of Selaginella lepidophylla in the Black Gap Area of the Chihuahuan Desert of Western Texas. The Southwestern Naturalist 37, 274–279. https://doi.org/10.2307/3671869

Wang, G., Wang, J., Zou, X., Chai, G., Wu, M., Wang, Z., 2019. Estimating the fractional cover of photosynthetic vegetation, non-photosynthetic vegetation and bare soil from MODIS data: Assessing the applicability of the NDVI-DFI model in the typical Xilingol grasslands. International Journal of Applied Earth Observation and Geoinformation 76, 154–166. https://doi.org/10.1016/j.jag.2018.11.006

Wang, L., Jiao, W., MacBean, N., Rulli, M.C., Manzoni, S., Vico, G., D'Odorico, P., 2022. Dryland productivity under a changing climate. Nat. Clim. Chang. 12, 981–994. https://doi.org/10.1038/s41558-022-01499-y

Yan, B., Wang, R., Gan, F., Wang, Z., 2010. Minerals mapping of the lunar surface with Clementine UVVIS/NIR data based on spectra unmixing method and Hapke model. Icarus 208, 11–19. https://doi.org/10.1016/j.icarus.2010.01.030